NASA/TM-20260001925

Measurement of Artificial and Real Bird Impact on a Very Rigid Flat Surface

J. Michael Pereira
Glenn Research Center, Cleveland, Ohio

Kevin L. Poormon
University of Dayton Research Institute, Dayton, Ohio

Stefan A. Ritt
German Aerospace Center DLR, Stuttgart, Germany

Wydo van de Waerdt
Fokker Aerostructures B.V., AN Hoogeveen, the Netherlands

Duane M. Revilock and James C. Akers
Glenn Research Center, Cleveland, Ohio

April 2026

NASA STI Program Report Series

Since its founding, NASA has been dedicated to the advancement of aeronautics and space science. The NASA scientific and technical information (STI) program plays a key part in helping NASA maintain this important role.

The NASA STI program operates under the auspices of the Agency Chief Information Officer. It collects, organizes, provides for archiving, and disseminates NASA's STI. The NASA STI program provides access to the NTRS Registered and its public interface, the NASA Technical Reports Server, thus providing one of the largest collections of aeronautical and space science STI in the world. Results are published in both non-NASA channels and by NASA in the NASA STI Report Series, which includes the following report types:

- TECHNICAL PUBLICATION.
  Reports of completed research or a major significant phase of research that present the results of NASA programs and include extensive data or theoretical analysis. Includes compilations of significant scientific and technical data and information deemed to be of continuing reference value. NASA counterpart of peer-reviewed formal professional papers but has less stringent limitations on manuscript length and extent of graphic presentations.

- TECHNICAL MEMORANDUM.
  Scientific and technical findings that are preliminary or of specialized interest, e.g., quick release reports, working papers, and bibliographies that contain minimal annotation. Does not contain extensive analysis.

- CONTRACTOR REPORT.
  Scientific and technical findings by NASA-sponsored contractors and grantees.

- CONFERENCE PUBLICATION.
  Collected papers from scientific and technical conferences, symposia, seminars, or other meetings sponsored or cosponsored by NASA.

- SPECIAL PUBLICATION.
  Scientific, technical, or historical information from NASA programs, projects, and missions, often concerned with subjects having substantial public interest.

- TECHNICAL TRANSLATION.
  English-language translations of foreign scientific and technical material pertinent to NASA's mission.

Specialized services also include organizing and publishing research results, distributing specialized research announcements and feeds, providing information desk and personal search support, and enabling data exchange services.

For more information about the NASA STI program, see the following:

- Access the NASA STI program home page at http://www.sti.nasa.gov

NASA/TM-20260001925

Measurement of Artificial and Real Bird Impact on a Very Rigid Flat Surface

J. Michael Pereira
Glenn Research Center, Cleveland, Ohio

Kevin L. Poormon
University of Dayton Research Institute, Dayton, Ohio

Stefan A. Ritt
German Aerospace Center DLR, Stuttgart, Germany

Wydo van de Waerdt
Fokker Aerostructures B.V., AN Hoogeveen, the Netherlands

Duane M. Revilock and James C. Akers
Glenn Research Center, Cleveland, Ohio

National Aeronautics and
Space Administration

Glenn Research Center
Cleveland, Ohio 44135

April 2026

Acknowledgments

The authors would like to acknowledge support from the NASA Revolutionary Vertical Lift Technology Project and institutional funding from the German Aerospace Center (DLR) under the Aeronautical Research Programme and from the German Federal Ministry of Defense.

This work was sponsored by the Advanced Air Vehicles Program at the NASA Glenn Research Center.

Level of Review: This material has been technically reviewed by technical management.

This report is available in electronic form at https://www.sti.nasa.gov/ and https://ntrs.nasa.gov/

NASA STI Program/Mail Stop 050
NASA Langley Research Center
Hampton, VA 23681-2199

Measurement of Artificial and Real Bird Impact on a Very Rigid Flat Surface

J. Michael Pereira*
National Aeronautics and Space Administration
Glenn Research Center
Cleveland, Ohio 44135

Kevin L. Poormon
University of Dayton Research Institute
Dayton, Ohio 45469

Stefan A. Ritt
German Aerospace Center DLR
70569 Stuttgart, Germany

Wydo van de Waerdt
Fokker Aerostructures B.V.
7903 AN Hoogeveen, the Netherlands

Duane M. Revilock and James C. Akers
National Aeronautics and Space Administration
Glenn Research Center
Cleveland, Ohio 44135

Introduction

Bird cadavers are used for development and certification testing of aircraft engines and structures to ensure that they can survive a bird strike during operation. The use of real birds has several disadvantages, including unsanitary test conditions, the need to euthanize animals, difficulty in procuring birds of the correct mass and species at arbitrary times of the year, and variability in test results due to bird-to-bird differences and the difficulty in launching an irregularly shaped projectile in a repeatable manner (Refs. 1 and 2). Artificial bird projectiles could overcome many of the disadvantages of real birds and may be acceptable to designers and certification authorities if they can be shown to produce a similar response to that of real birds. This has led to the investigation of artificial bird materials that can be used in lieu of real birds that would produce the same damage and response in aircraft structures as real birds.

A number of artificial bird designs have been proposed, some of a homogeneous design based on ballistic gelatin or other soft materials (Refs. 2 and 5). An artificial bird developed by the German Aerospace Center, DLR, incorporates a plastic shell and ribs, filled with a ballistic gel mixture (Ref. 6). Like others, it can be manufactured in various shapes, such as a regular cylinder with a spherical front discussed in this report, or an ellipsoidal shape as was used in a research study on stabilizer leading edges (Ref. 7). The German company Crashtest-Service (CTS) has developed a realistic-looking artificial bird projectile that has many of the physical features of a real bird, including artificial bones and flesh (Ref. 8).

*Retired.

A small study compared the DLR artificial bird with the CTS artificial bird in terms of load pulses using piezoelectric load cells (Ref. 9).

Demonstrating the similarity in damage production and response between artificial bird projectiles and real birds has been a challenge, in part due to the lack of real bird data needed for a comparison. Numerous researchers have proposed a number of different methods to measure and compare the impact response of soft materials, such as real birds and artificial bird projectiles, including the use of a Hopkinson bar or tube (Refs. 10 to 13), shock measurements in flyer plate tests (Ref. 14), and compliant targets (Ref. 10).

For this study, impact tests were conducted with real chicken and duck cadavers and two types of artificial bird projectiles utilizing a large-diameter Hopkinson bar. The objectives were to compare the impact forces generated by the different projectiles, to provide real bird data for comparison with other proposed artificial bird projectiles, and to provide data for the development of computational impact models of real bird and artificial bird projectiles. The testing was conducted in conformance with the SAE AS6940 test standard (Ref. 15). This report describes the methods used in testing, the force measurements obtained directly from strain measurements on the Hopkinson bar, and still images from high-speed videos of the test, which are useful for understanding and interpreting the measured force results. A future publication will present results of additional force measurements computed from particle velocities at the end of the bar, an analysis of the effects of the filtering on the results, and the calculations of energy spectral densities to understand the frequency content of the results.

Methods

Impact tests were conducted by launching projectiles axially into a large-diameter Hopkinson bar using a compressed air gas gun. The intent was to shoot the projectile so that it impacted in an axial orientation with no pitch or yaw. Twenty-nine tests were conducted using real birds and two types of artificial bird projectiles at three nominal velocities of 50, 110, and 310 m/s. The tests were conducted at the University of Dayton Research Institute (UDRI) Impact Physics Laboratory. A report summarizing the test procedures is available in Reference 16.

Projectiles

The three types of projectiles were chicken and duck cadavers, an artificial bird projectile manufactured by UDRI prior to each test, and a proprietary artificial bird projectile provided by the German Aerospace Center, DLR.

The bird cadavers were received in a frozen state and thawed prior to testing. They were 1.8-kg (4-lb) Golden Comet chickens and 1-kg (2.2-lb) Mallard ducks that were prepared per ASTM F330-21 (Ref. 17). The original bird weight was within 10% of the final weight required by ASTM F330. The bird weight was adjusted by injecting a small amount of water into the bird if it was under the desired mass or trimming off pieces of the wings and legs if it was over. The density of the bird cadavers was not measured. The bird was placed inside a sewn muslin cloth bag weighing approximately 16 g (0.036 lb) for the 1.8-kg bird and 13 g (0.029 lb) for the 1-kg bird. After recording the final weight (bird plus bag) the projectile was inserted into a sabot which was loaded into the gun barrel. During the launch process, the sabot was stripped off near the muzzle of the gun and contained in the gun's sabot stripper section allowing only the projectile to travel to the target.

The UDRI soft body artificial bird projectiles were cylindrical in shape with a hemispherical nose and weighed nominally 1 kg (2.2-lb) or 1.8 kg (4-lb). These projectiles were fabricated from a mixture of water and gelatin with the density controlled by the addition of phenolic microballoons. The density of

these artificial bird projectiles was nominally 0.95 g/cc (0.034 lb/in^3), which is approximately the same as that of a chicken (Ref. 10). The 1.8-kg projectile had a nominal diameter of 107 mm (4.2 in.) and overall length of 234 mm (9.2 in.). The 1-kg (2.2-lb) projectiles had a nominal diameter of 96.5 mm (3.80 in.) and overall length of 161 mm (6.34 in.). These artificial bird projectile weights were adjusted to be close to the target weight by trimming off material at the flat rear end of the projectile. Weight measurements were obtained using an Ohaus balance with a resolution of 0.45 g (0.001 lb). The UDRI gelatin artificial bird projectiles were near room temperature when launched (~19 °C, ~67 °F).

The DLR artificial bird projectiles were a proprietary gelatin mixture encased in a thin 3D-printed plastic shell with internal ribbing (Ref. 6). The 1.8-kg DLR projectiles had a nominal diameter of 107 mm (4.2 in.) and a length of 232 mm (9.12 in.). The shape was patterned after the UDRI gelatin projectiles, with a hemispherical nose and a flat back. The 1-kg DLR projectiles had a nominal diameter of 96.5 mm (3.80 in.) and an overall length of 193 mm (7.6 in.) with both ends being hemispherical. The nominally 1-kg DLR projectiles had an actual mass of approximately 1.18 kg (2.6 lbm). The DLR projectiles were stored in a refrigerator at 4.4 °C (40 °F) and were tested cold at nominally 10 °C (50 °F).

Test Conduction

Three impact tests were conducted for each projectile at each velocity, with the exception of the 50 m/s tests with the UDRI artificial bird projectile, where five tests were conducted, the first of which provided no force data due to a triggering issue. The projectiles were launched using a compressed air gas gun with a smooth bore of 178 mm (7 in.) and a length of 9 m (30 ft) with a tapered-diameter sabot stripper attached to the muzzle of the barrel (Figure 1). The projectile was installed in a standard one-piece cast polyurethane sabot with a cavity sized to fit the projectile being launched. Additional details regarding the gun and the sabot are given in Reference 16.

Figure 1.—Gas gun used for launching projectiles.

Force Measurement Using Strain Gages

The projectiles were impacted onto a large-diameter Al6061 cylindrical Hopkinson bar with a diameter of 305 mm (12 in.). The impact direction was normal to the flat front face of the bar. Figure 2 shows the location of the Hopkinson bar relative to the tapered section of the gun barrel. The bar consisted of two sections, each 3.65 m (12 ft) long with machined faces and supported on rubber rollers so that they were in direct contact with each other. Ultrasound gel was placed between the two sections in an attempt to ensure full wave transmission at the interface. The overall length of the bar (7.3 m) was selected so that impacts at low velocities (50 m/s) would be complete before reflections from the end of the bar affected the force measurements. Unfortunately, full wave transmission did not occur between the two Hopkinson bar sections, as will be discussed. Therefore, only the first ~1.2 ms of force response was unaffected by wave reflections from the interface of the two Hopkinson bar sections. The test method is described in Reference 15, and a detailed analysis of the test method is given in Reference 12.

The bar was instrumented with strain gages at two locations, 457.2 and 609.6 mm (1.5 and 2 diameters) from the impacted face, referred to here as bridge locations 1 and 2, respectively. Schematics of the Hopkinson bar and instrumentation layout are shown in Figures 3 and 4.

Figure 2.—Location of Hopkinson bar (center) relative to tapered section of gun barrel (left).

Figure 3.—Schematic of two-section Hopkinson bar showing projectile on left.

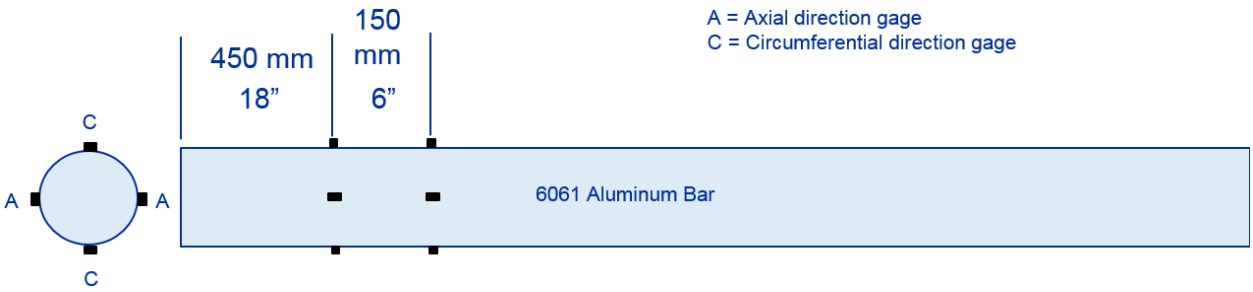

Figure 4.—Schematic of first section of Hopkinson bar showing strain gage locations.

Strain time histories were recorded near the impact end of the Hopkinson bar at the locations shown in Figure 4 at a sampling rate of 1.25×10^6 samples/s. Because of the very large diameter of the Hopkinson bar, overall strain levels were quite low, on the order of 200 με or less at the highest impact velocities. Semiconductor strain gages were utilized to allow the measurement of the very low strain levels. The strain gages were in a full bridge configuration with two axial gages, 180° apart, and two circumferential gages equally spaced in between for bridge completion. The strain was calculated using Equation (1).

$$\epsilon = \frac{2\Delta V_m}{V_e S_g (1+\nu)} \tag{1}$$

where ΔV_m is the change in measured voltage, which was offset to zero prior to each test, V_e is the excitation voltage (7 V), S_g is the gage factor (162), and ν is Poisson's ratio of Al6061 (0.33).

The average stress, σ, in the bar was computed from the product of the average strain, ϵ, and the modulus of elasticity, E, as shown in Equation (2).

$$\sigma = E\epsilon \tag{2}$$

The force in the bar was calculated from the product of the average stress and the cross-sectional area of the bar.

As previously mentioned, full wave transmission across the interface of the two bars did not occur and resulted in reflected waves returning to the measurement locations at approximately 1.2 ms after impact. Therefore, only the first 1.2 ms of strain time histories were processed and the corresponding force time histories presented here. The full impact force signals were complete in this time period for the highest velocity impact tests (nominally 300 m/s). For the lower velocity tests, the impact force duration was longer than 1.2 ms. and, therefore, only the initial portion of the force history is presented. However, the data in this time duration are useful for all tests.

As discussed in Reference 12, the data at frequencies above 8 to 10 kHz are not representative of the average force in the bar due to nonplanar response and dispersion effects at higher frequencies. Therefore, the strain data were low-pass filtered using a four-pole digital Butterworth low-pass filter with a cutoff frequency of 10 kHz. To increase the steepness of the rolloff of this lowpass filter and to eliminate phase distortion, the strain signals were passed forwards and backwards through this filter.

High-Speed Video

Three Phantom® (Vision Research Inc.) V2012 digital high-speed cameras were used to record the impact events. The cameras recorded the 50 and 110 m/s tests with a framing rate of 10,000 frames per second (fps). The framing rate for the 310 m/s tests was 20,000 fps. These framing rates were sufficient to

examine the impact and projectile fragmentation pattern during the test. One camera was positioned to view the impact from the side. A 304.8-mm (12-in.) square reference grid was placed behind the test article for reference. The side camera's sensor plane was 255.3 cm (100.5 in.) from the gun center line and 358.1 cm (141.0 in.) from the reference grid. The second camera was positioned to view the impact from the above. A 304.8-mm (12-in.) square reference grid was placed behind the test article for reference. The top camera's sensor plane was 213.4 cm (84 in.) from the gun center line and 328.9 cm (129.5 in) from the reference grid. The third camera was positioned alongside the gun barrel and viewed the front face of the Hopkinson bar.

Test Details

Twenty-nine impact tests were conducted. All tests were performed at room temperature (19 ± 1 °C). Table 1 gives a summary of the impact conditions, including projectile mass, dimensions, density (where measured) and impact velocity. In the first test conducted, 5-3324, the data acquisition system did not trigger and no strain results were obtained.

TABLE 1.—SUMMARY OF TESTS

Shot no.	Projectile	Projectile mass, kg	Projectile diameter, mm	Projectile length, mm	Projectile density, g/cc	Impact velocity, m/s	Comments
5-3324	UDRI	1.008	96.5	161.3	0.949	52.7	Projectile flattened on impact and rebounded in one piece.
5-3325	UDRI	1.008	96.5	161.3	0.949	49.1	Projectile flattened on impact and rebounded in one piece.
5-3326	UDRI	1.009	96.5	161.3	0.949	49.4	Projectile flattened on impact and rebounded in one piece.
5-3327	UDRI	1.009	96.5	161.3	0.949	49.7	Projectile flattened on impact and rebounded in one piece.
5-3328	UDRI	1.006	96.5	161.3	0.947	49.1	Projectile flattened on impact and rebounded in one piece.
5-3329	UDRI	1.823	106.7	233.7	0.944	110.9	Projectile flattened on impact and tore into longitudinal segments spreading out radially across the bar face. Most of the segments remained attached at the back of the projectile. Projectile found lying on floor in front of bar largely in one piece.
5-3330	UDRI	1.821	106.7	232.4	0.949	110	Projectile flattened on impact and tore into longitudinal segments spreading out radially across the bar face. Most of the segments remained attached at the back of the projectile. Projectile found lying on floor in front of bar largely in one piece.
5-3331	UDRI	1.818	106.7	238.0	0.923	110.6	Projectile flattened on impact and tore into longitudinal segments spreading out radially across the bar face. Most of the segments remained attached at the back of the projectile. Projectile found lying on floor in front of bar largely in one piece.
5-3332	UDRI	1.819	106.7	237.5	0.926	310.9	Projectile flattened on impact into a thin layer spreading out radially across the bar face. Projectile found fragmented into many small pieces.

TABLE 1.—SUMMARY OF TESTS

Shot no.	Projectile	Projectile mass, kg	Projectile diameter, mm	Projectile length, mm	Projectile density, g/cc	Impact velocity, m/s	Comments
5-3333	UDRI	1.820	106.7	231.1	0.954	310.3	Projectile flattened on impact into a thin layer spreading out radially across the bar face. Projectile found fragmented into many small pieces.
5-3334	UDRI	1.818	106.7	231.1	0.953	311.9	Projectile flattened on impact into a thin layer spreading out radially across the bar face. Projectile found fragmented into many small pieces.
5-3368	Duck	0.998	95-100	191	-------	49.3	Bird flattened on impact and rebounded in one piece. Blood/fluid squirted out.
5-3369	Duck	1.003	95-100	191	-------	50.2	Bird flattened on impact and rebounded in several large pieces. Blood/fluid squirted out.
5-3370	Duck	1.004	95-100	191	-------	49.3	Bird flattened on impact and rebounded in 2 large pieces. Blood/fluid squirted out.
5-3371	Chicken	1.817	115-130	216	-------	109.8	Bird flattened on impact and fragmented radially into many pieces.
5-3372	Chicken	1.819	115-130	216	-------	107.5	Bird flattened on impact and fragmented radially into many pieces.
5-3373	Chicken	1.816	115-130	216	-------	110.3	Bird flattened on impact and fragmented radially into many pieces.
5-3374	Chicken	1.817	115-130	216	-------	308.9	Bird flattened on impact and fragmented radially into many small pieces.
5-3375	Chicken	1.820	115-130	216	-------	309	Bird flattened on impact and fragmented radially into many small pieces.
5-3376	Chicken	1.816	115-130	216	-------	309.6	Bird flattened on impact and fragmented radially into many small pieces.
5-3377	DLR	1.840	106.4	231.6	0.967	103.3	Projectile flattened on impact and fragmented radially into many pieces.
5-3378	DLR	1.828	106.4	231.6	0.96	117.3	Projectile flattened on impact and fragmented radially into many pieces.
5-3379	DLR	1.845	106.4	231.6	0.969	111.2	Projectile flattened on impact and fragmented radially into many pieces.
5-3380	DLR	1.179	96.6	193.0	0.999	50.6	Projectile flattened on impact and fragmented radially into pieces, some large.
5-3381	DLR	1.181	96.5	193.0	1.004	48.9	Projectile flattened on impact and fragmented radially into pieces.
5-3382	DLR	1.177	96.5	193.0	1.004	48.5	Projectile flattened on impact and fragmented radially into pieces.
5-3383	DLR	1.828	106.4	231.6	0.96	299.8	Projectile flattened on impact and spread radially into paste-like consistency.
5-3384	DLR	1.817	106.4	231.6	0.955	310.9	Projectile flattened on impact and spread radially into paste-like consistency.
5-3385	DLR	1.846	106.4	231.6	0.97	312.3	Projectile flattened on impact and spread radially into paste-like consistency.

Results

Still images from the upper and side high-speed video cameras, showing a frame directly before impact, are presented in Appendix A. Review of the images shows that for all three types of bird projectiles, there was significant yaw and pitch misalignment at the lowest impact velocity. In general, for the intermediate impact velocity of nominally 110 m/s, the yaw and pitch orientations were acceptable, but there was some elongation of the UDRI artificial bird projectiles and some cracking of the outer plastic skin in the DLR artificial projectiles due to the higher accelerations. For the highest impact velocities of nominally 310 m/s impact, while the yaw and pitch orientations were generally acceptable, there was significant elongation in the UDRI artificial bird projectiles and significant fracturing and elongation in the DLR artificial bird projectiles.

The impact force time histories on the end of the Hopkinson bar, calculated from the measured strain time histories in strain bridge 1, are presented in Figures 5 to 7 for the nominally 50, 110, and 310 m/s tests, respectively. The impact force time histories calculated from the measured strain time histories in strain bridge 2 were similar to those of strain bridge 1 for all tests, but slightly offset in time due to the wave transmission speed. The impact force time histories only have frequency content up to 10 kHz due to the lowpass filtering of the strain time histories. As mentioned, due to reflections returning from the interface between the two bars, most tests were conducted using only the first section of the bar. The reflections occurred at a time slightly greater than 1.2 ms. This was long enough to capture the full impact force time histories for the 310 m/s velocity impact tests (i.e., forces start and end at zero) but was not long enough to for the impact forces to return to zero for the lower velocity impact tests. In the figures, the abscissa has a range of 0 to 1.2 ms.

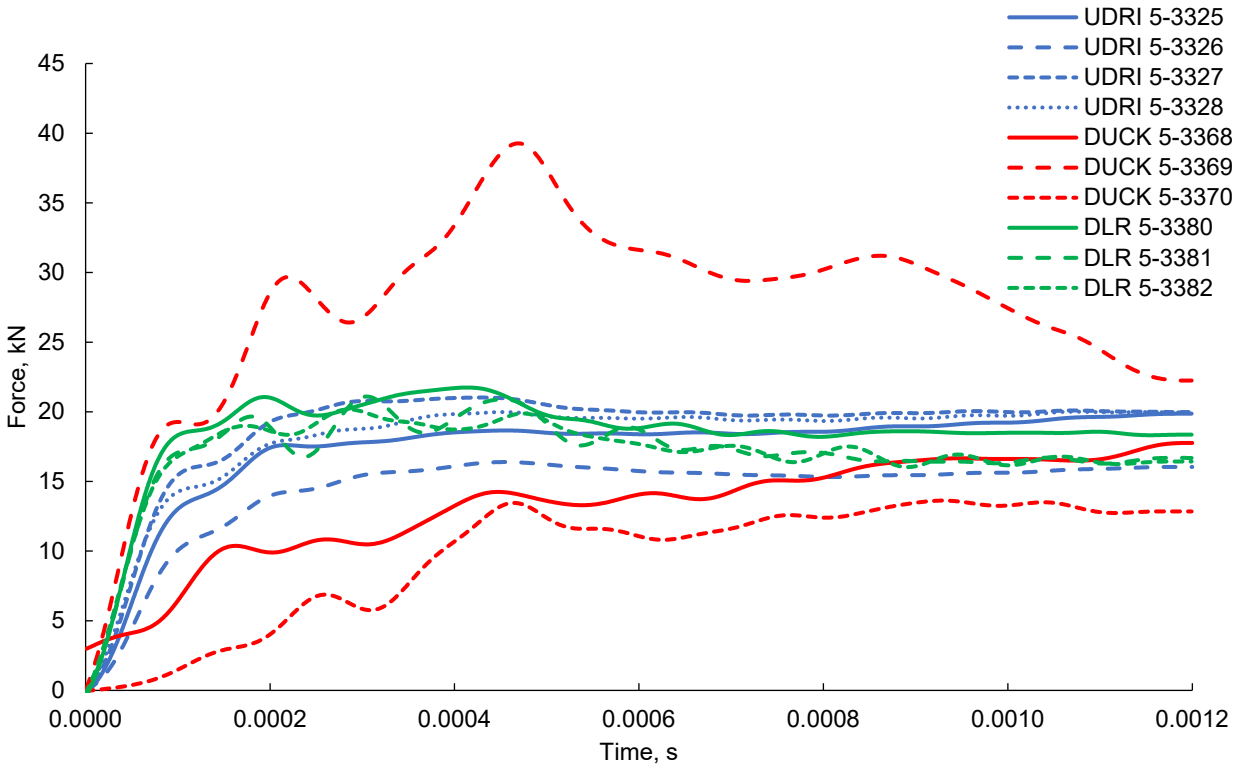

Figure 5.—Impact forces from 1-kg projectiles at nominally 50 m/s.

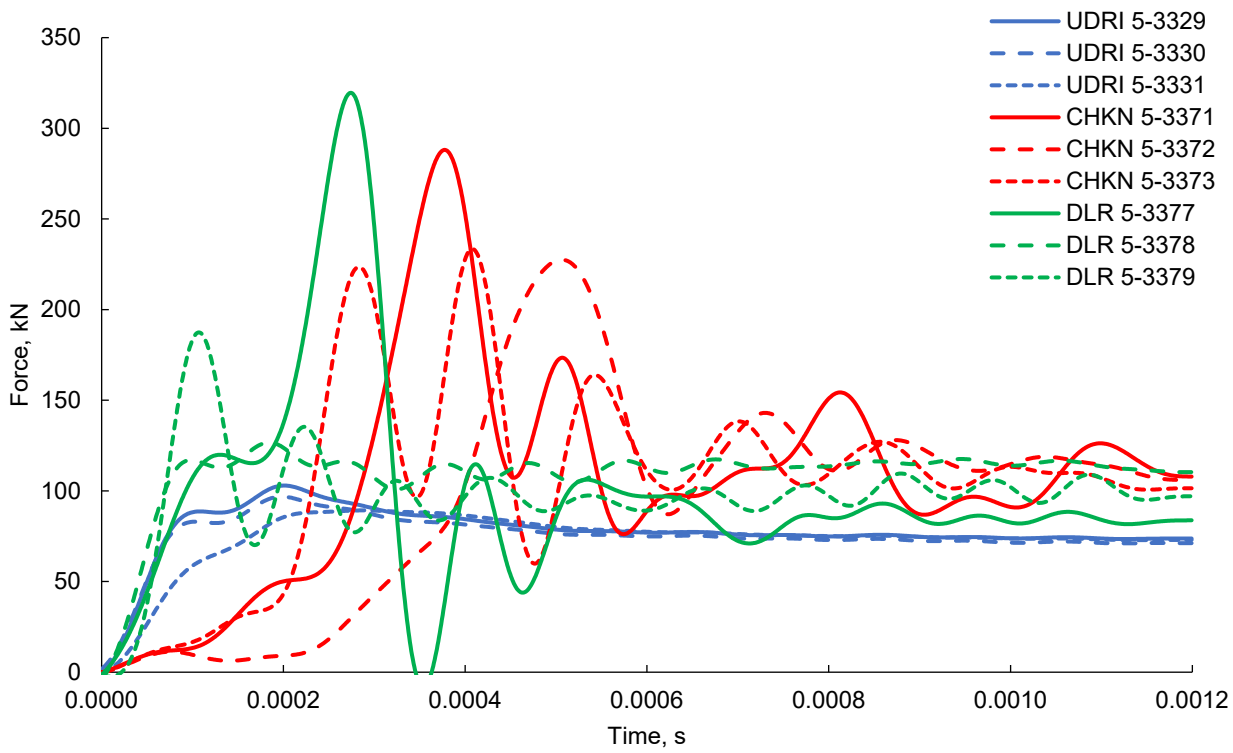

Figure 6.—Impact forces from 1.8-kg projectiles at nominally 110 m/s.

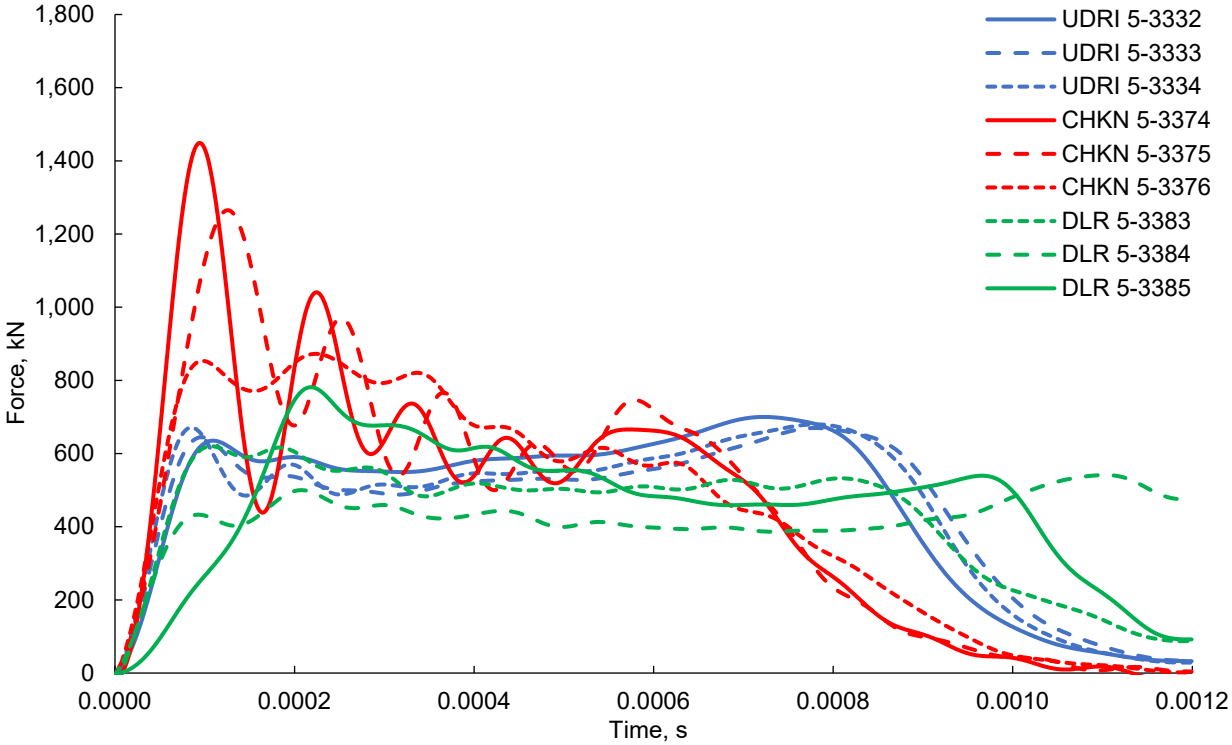

Figure 7.—Impact forces from 1.8-kg projectiles at nominally 310 m/s.

Discussion and Conclusions

Average impact forces ranged from on the order of 20 to 800 kN over the velocity range. In general, the forces showed transient behavior at the beginning of the time duration and then settled into a steady-state response at the end of the recorded period. The impact force measurements for the two types of artificial bird projectiles were more repeatable than those for the real bird projectiles, with the exception of test 5-3377 involving a DLR artificial projectile at an impact velocity of 103.3 m/s. Much of the nonrepeatability in the test results can be explained by observing the orientations, shape, and makeup of the projectiles at impact, shown in Appendix A. A number of variables can affect the initial transient behavior and quasi-steady-state response. The real bird projectiles and DLR artificial bird projectiles generally showed higher frequency components in their impact forces. This may be attributed to local inhomogeneities due, for example, to bones and plastic reinforcement (Ref. 18).

The impact force initial short duration transient behavior and subsequent quasi-steady-state response have been observed in other studies and have been attributed to shock pressures developing during the initial impact followed by release waves propagating from the free surfaces (Ref. 19). This behavior is less evident in oblique impacts or impacts where the front surface of the projectile is not flat. The initial short-duration transient behavior is more prominent in tests where a flatter front face of the projectile is presented, such as in tests 5-3371, 5-3372, 5-3373, 5-3377 (Figure 6) and 5-3374 and 5-3375 (Figure 7). The impact orientations of the projectiles for these tests can be seen in Appendix A .

The impact force is highly dependent on the impact velocity, density, and orientation of the projectile at impact. The effects of orientation on the impact force is particularly apparent when comparing tests 5-3369 and 5-3370 (Figure 5). As can be seen in Appendix A, the projectile in test 5-3369 impacted in an almost flatwise orientation, resulting in a significantly higher force than that in test 5-3370. Much of the nonrepeatability in the tests can be attributed to the effects of projectile orientation at impact. These effects will be discussed in more detail in a future publication.

Apart from the impact force initial short-duration transient response and the nonrepeatability, particularly in real bird tests, due to factors that can be partially explained by impact orientations, there was quite good subjective agreement in the overall forces from the three types of projectiles. It should be noted that in an actual bird impact on a transparency, leading edge, or fan blade, the impact is unlikely to involve a flat-faced bird impacting a rigid flat object in a normal direction. Therefore, in real world applications, the transients caused by initial shock pressure and release may be less of a factor in the transmitted force.

Appendix A.—Still Images From High-Speed Video Cameras

Figures A.1 to A.56 show impact orientations of the projectiles for these tests.

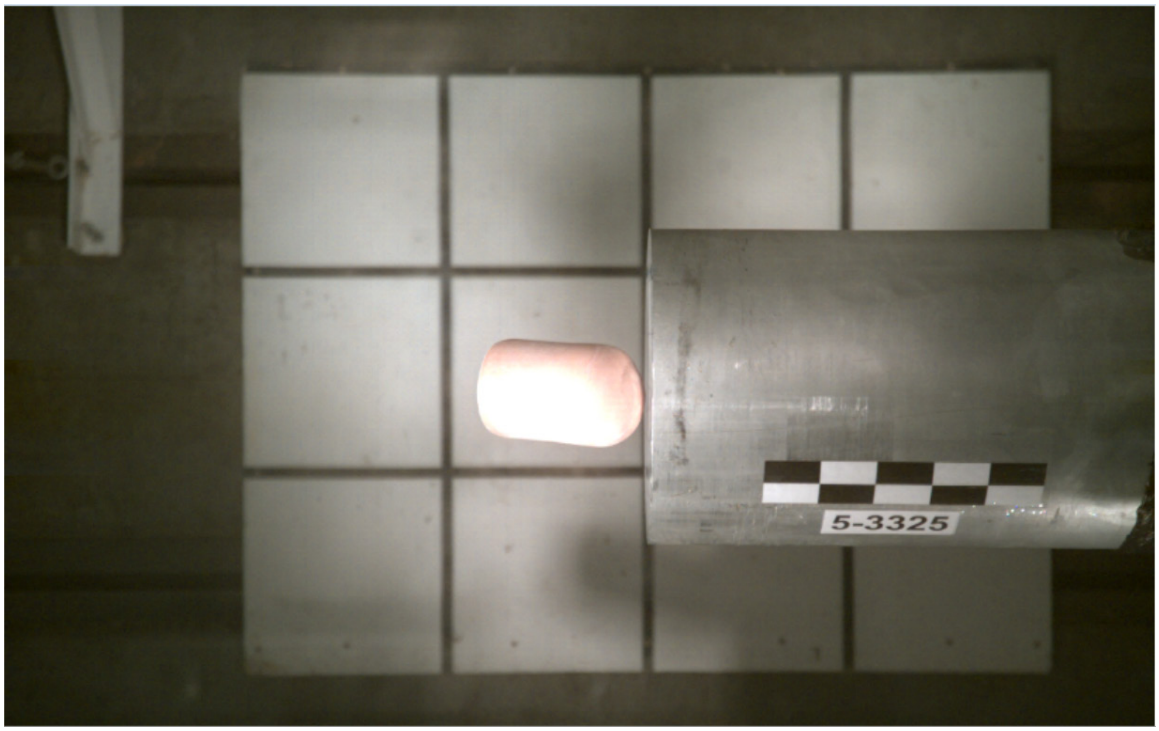

Figure A.1.—Image 5-3325 top view.

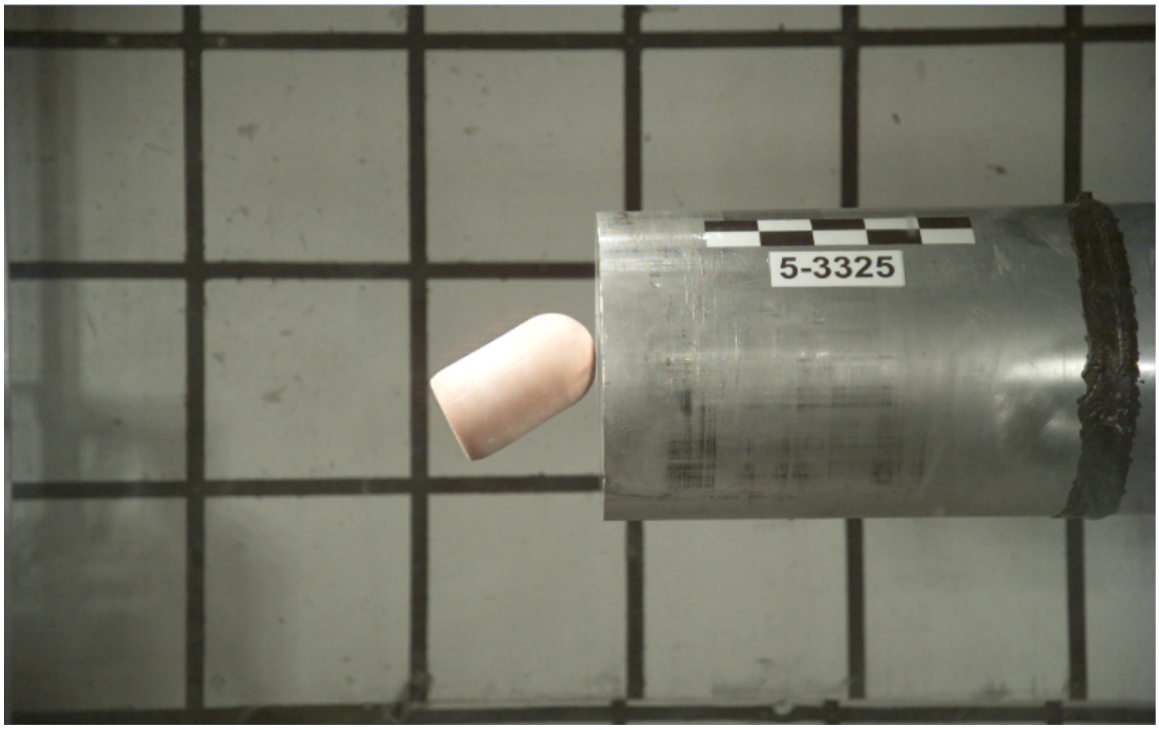

Figure A.2.—Image 5-3325 side view.

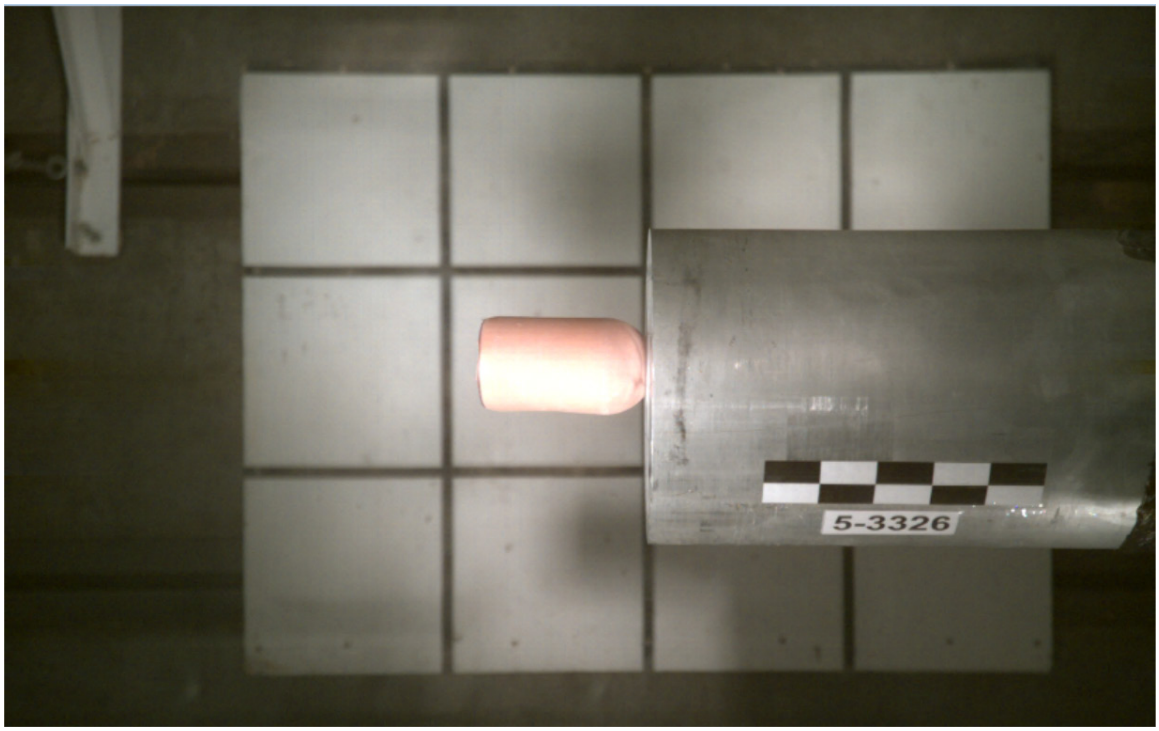

Figure A.3.—Image 5-3326 top view.

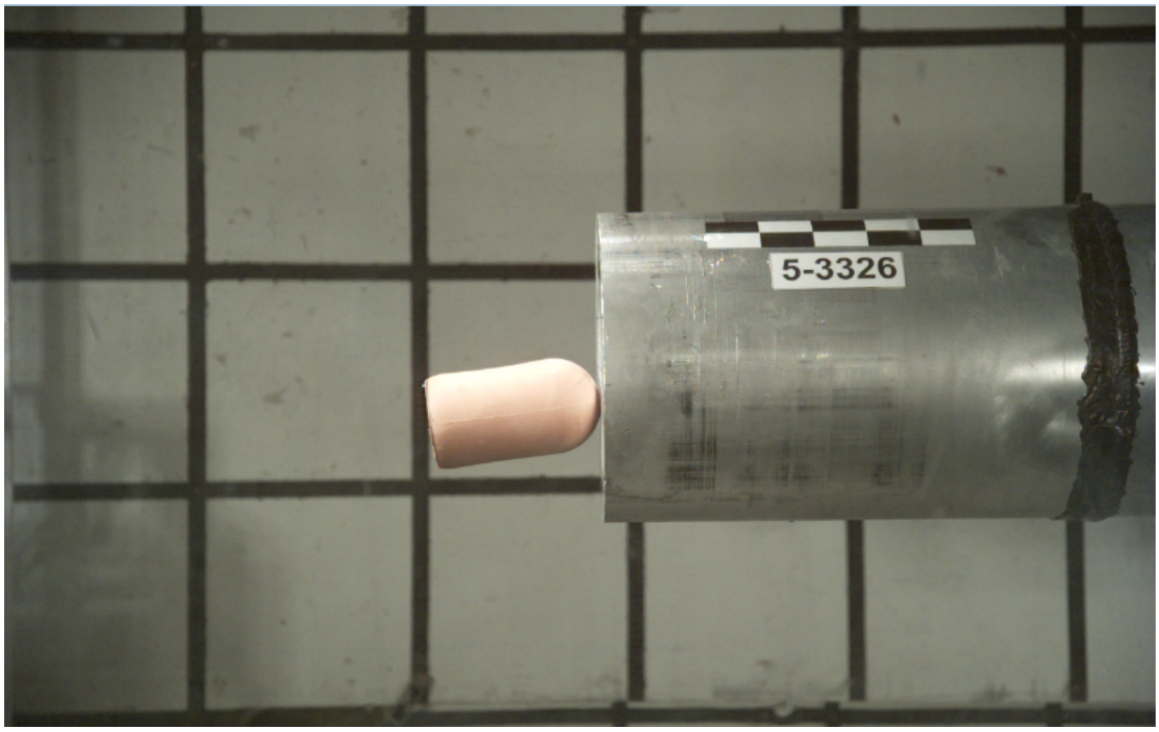

Figure A.4.—Image 5-3326 side view.

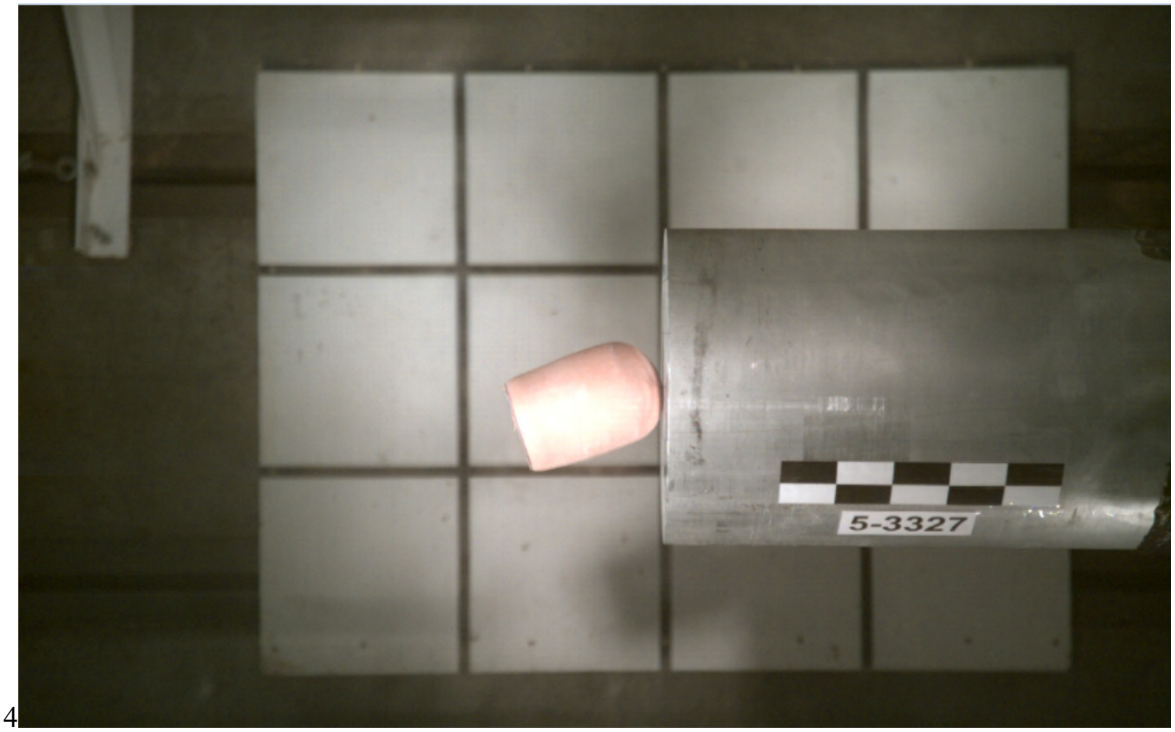

Figure A.5.—Image 5-3327 top view.

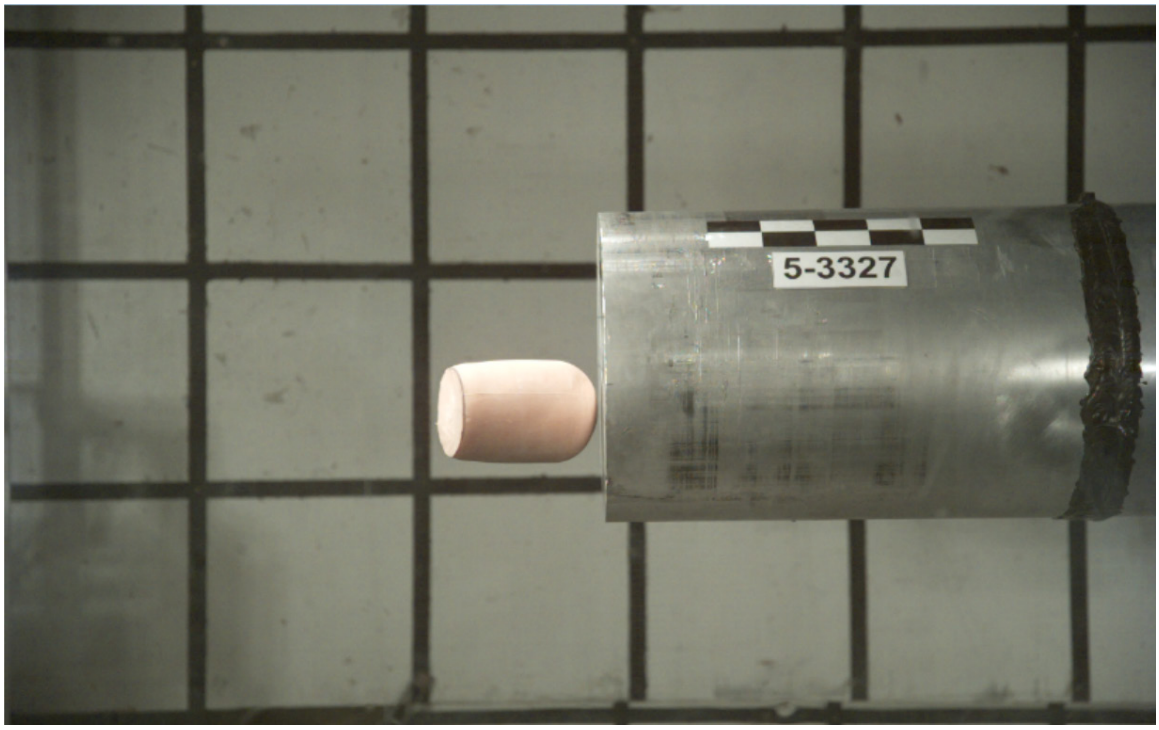

Figure A.6.—Image 5-3327 side view.

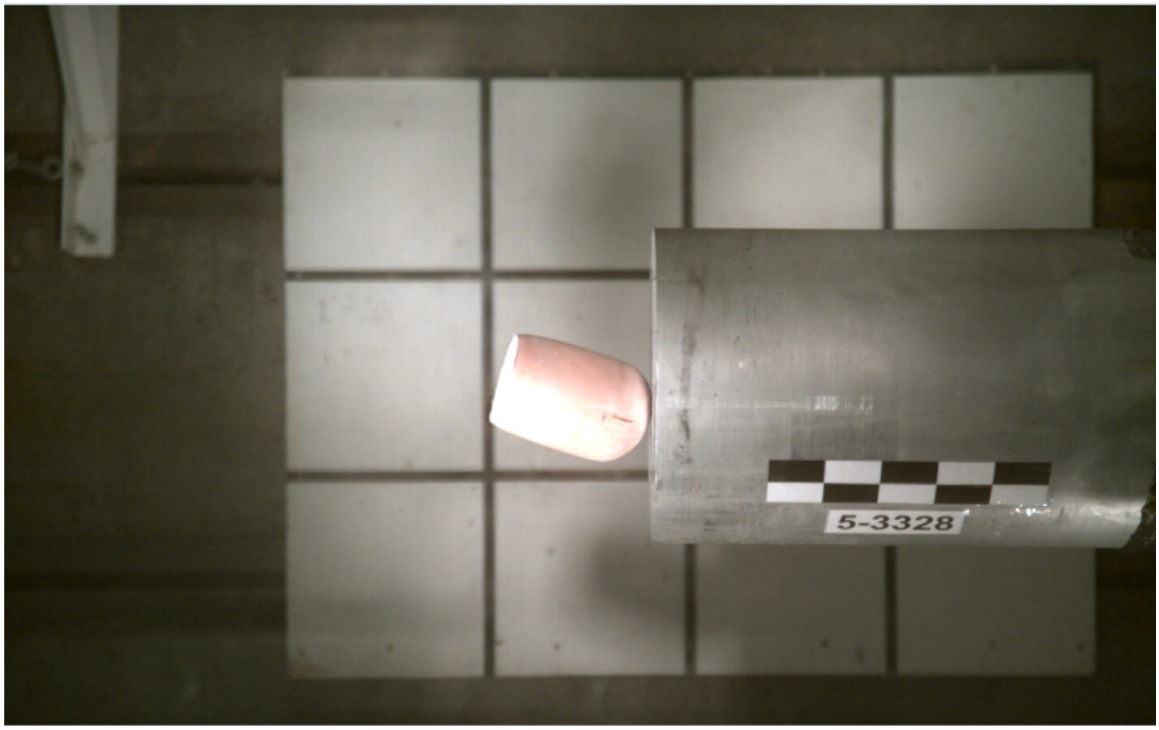

Figure A.7.—Image 5-3328 top view.

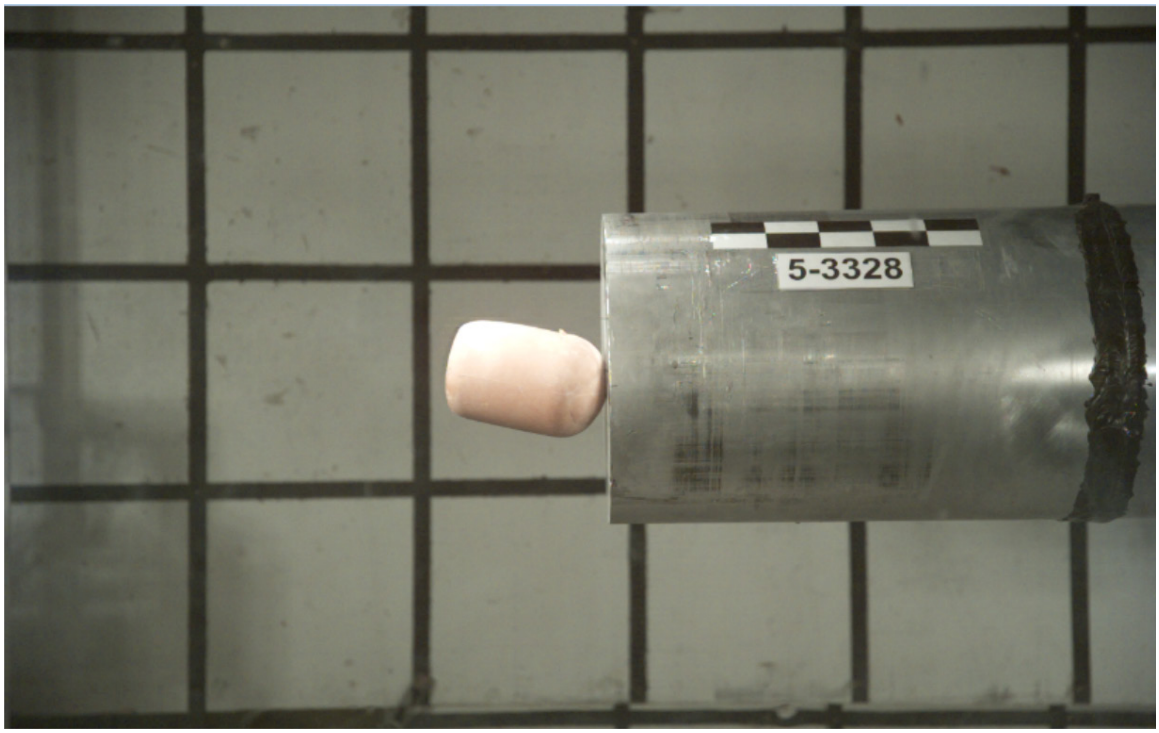

Figure A.8.—Image 5-3328 side view.

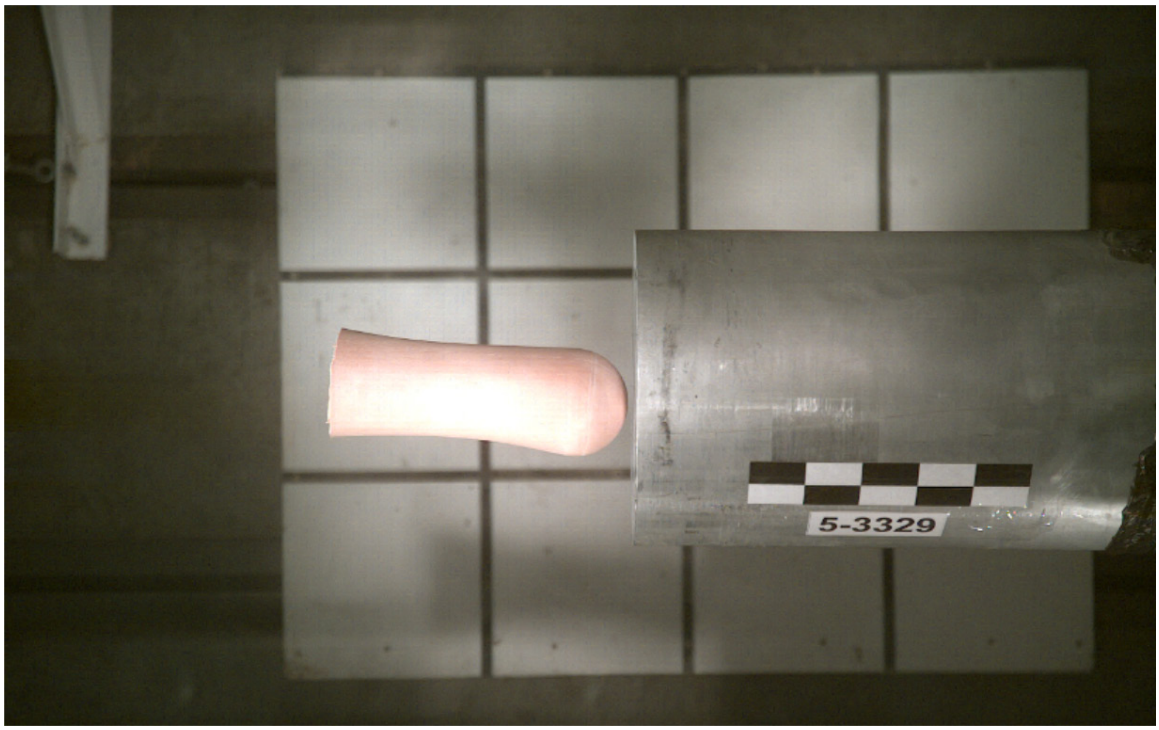

Figure A.9.—Image 5-3329 top view.

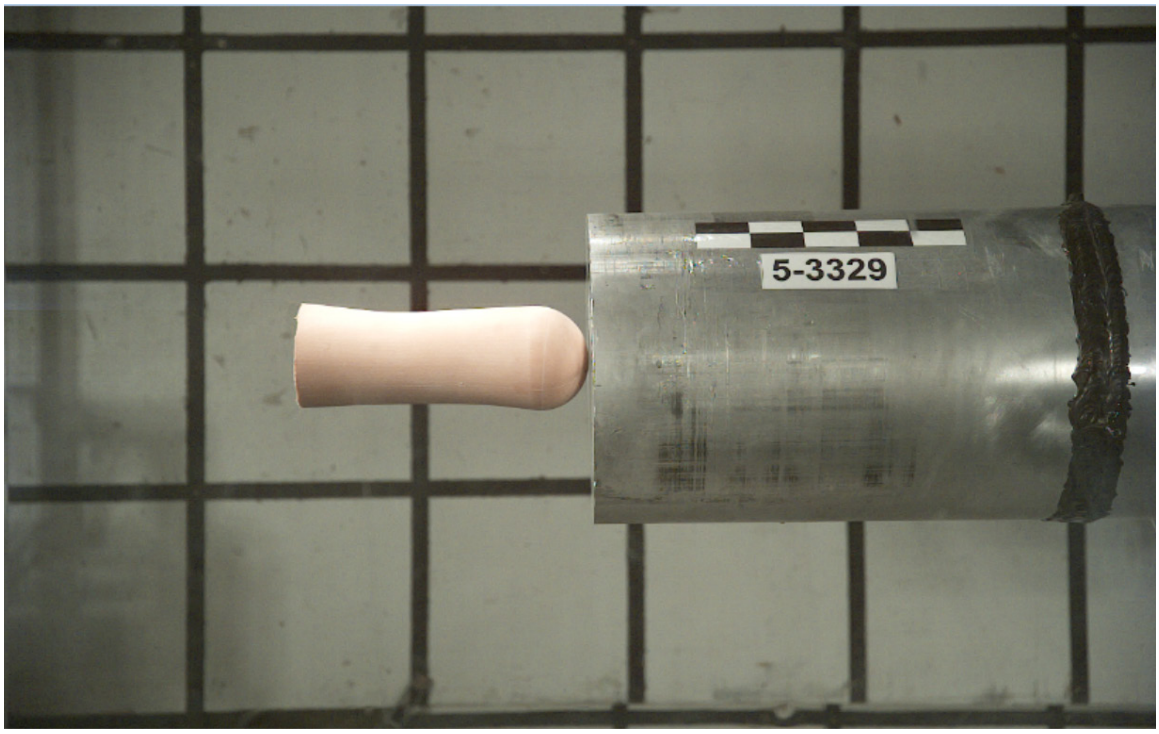

Figure A.10.—Image 5-3329 side view.

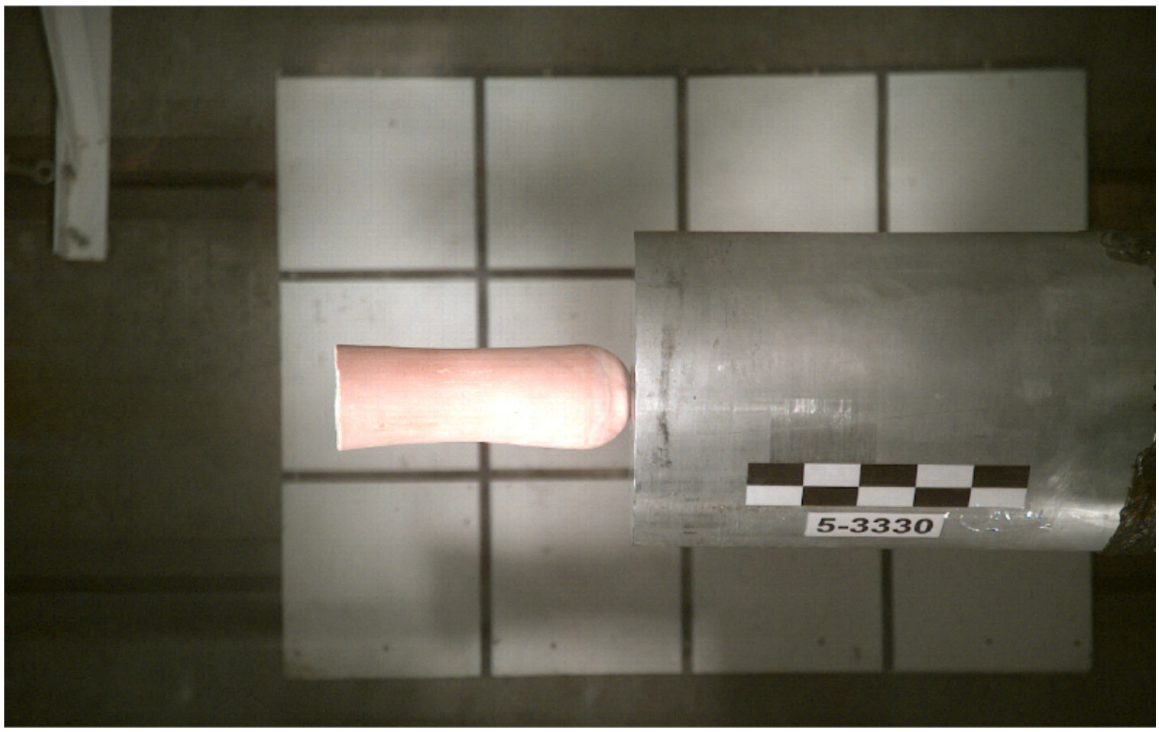

Figure A.11.—Image 5-3330 top view.

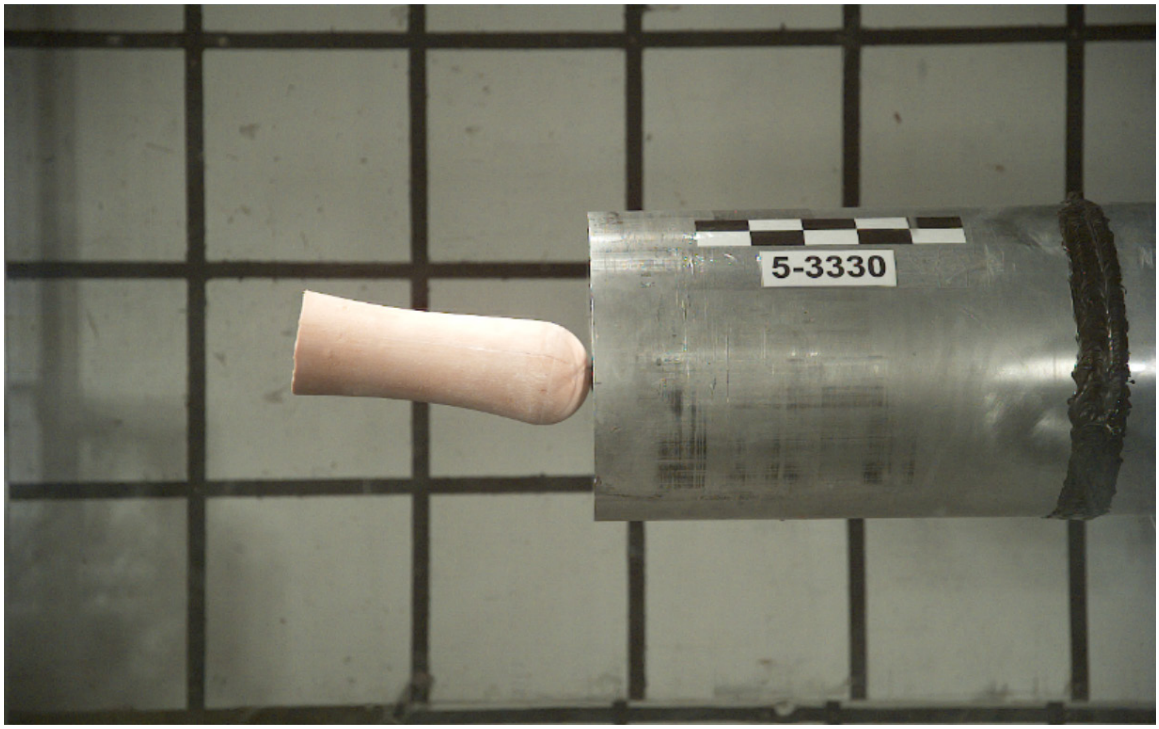

Figure A.12.—Image 5-3330 side view.

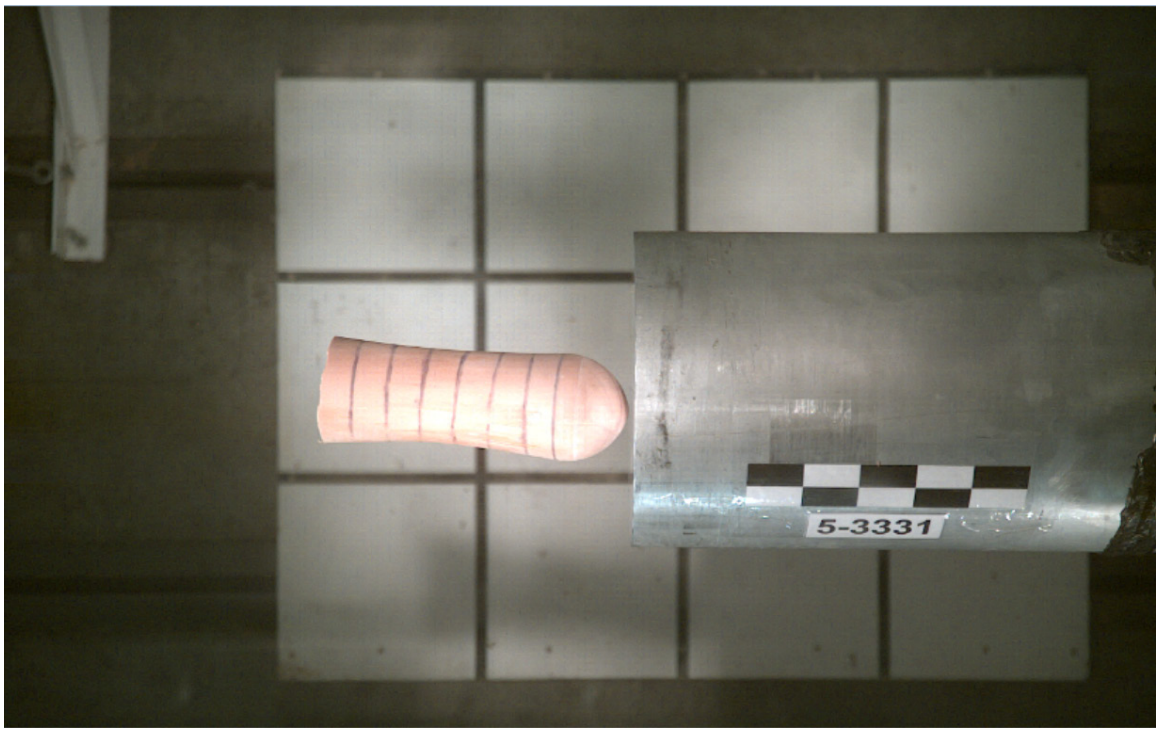

Figure A.13.—Image 5-3331 top view.

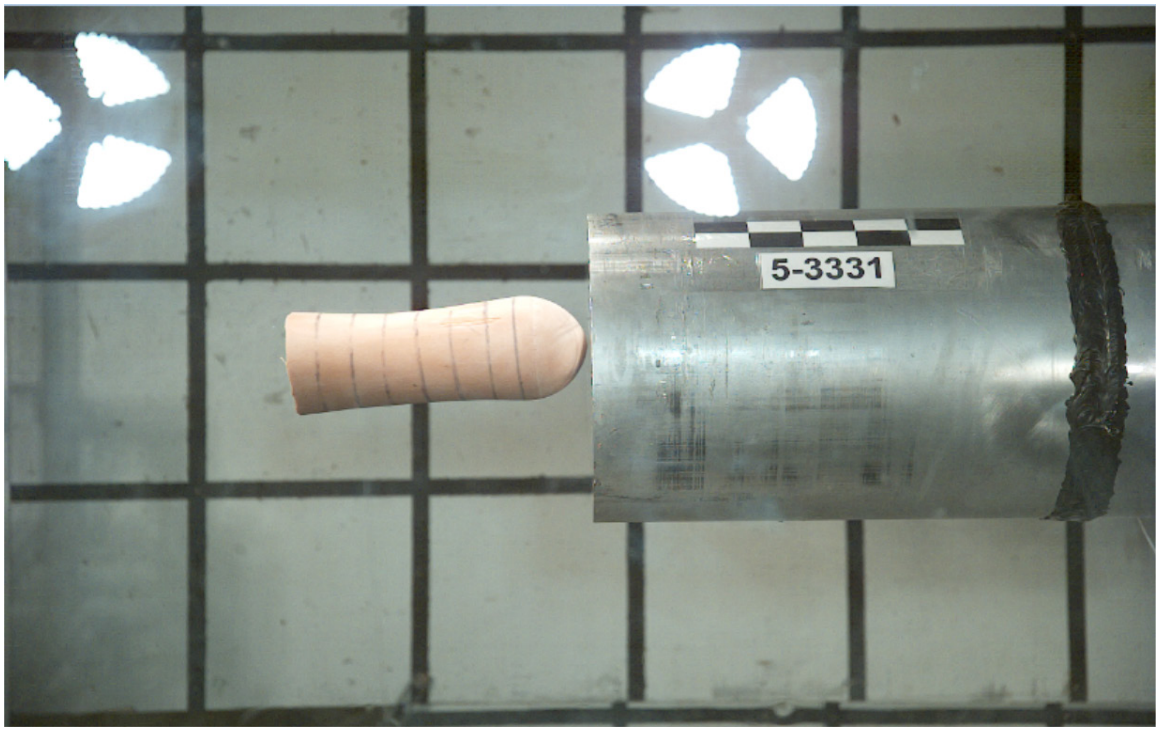

Figure A.14.—Image 5-3331 side view.

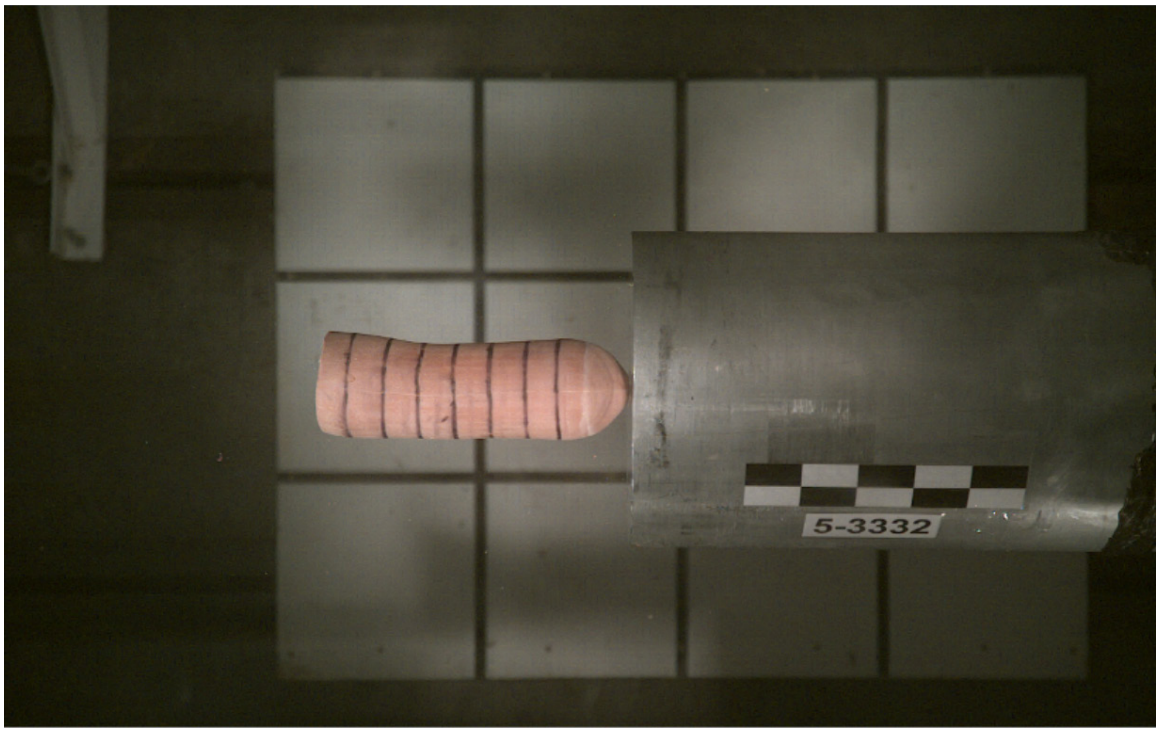

Figure A.15.—Image 5-3332 top view.

Figure A.16.—Image 5-3332 side view.

Figure A.17.—Image 5-3333 top view.

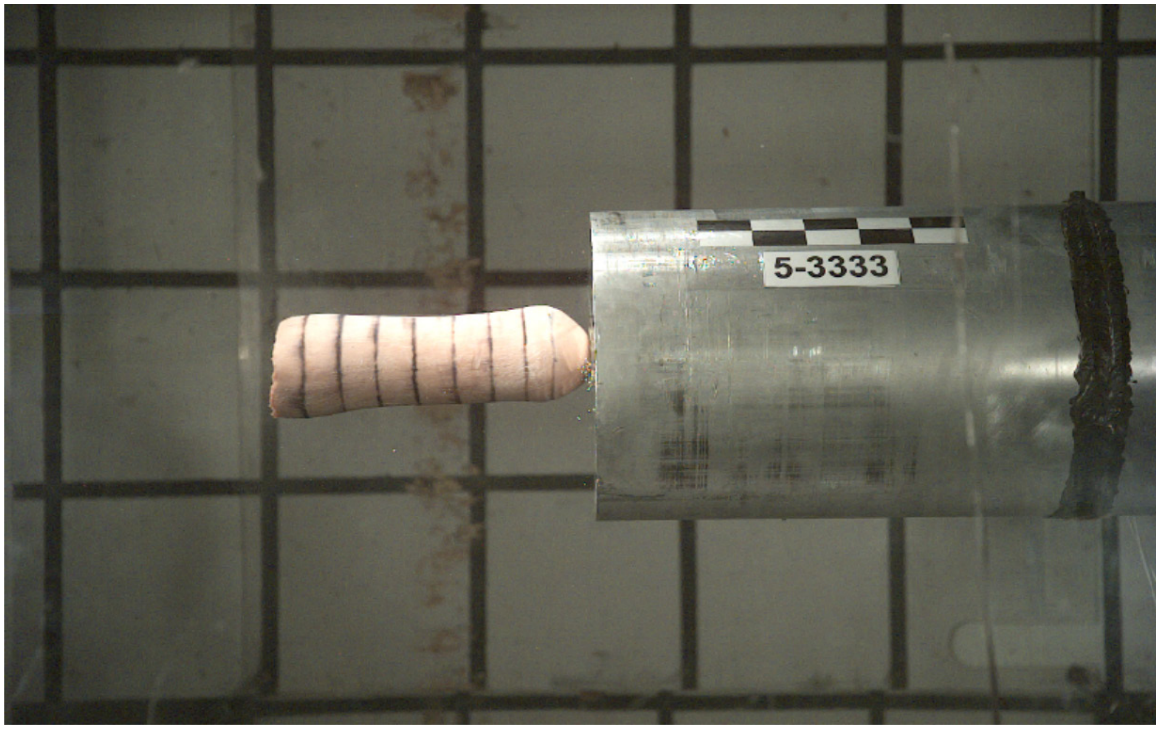

Figure A.18.—Image 5-3333 side view.

Figure A.19.—Image 5-3334 top view.

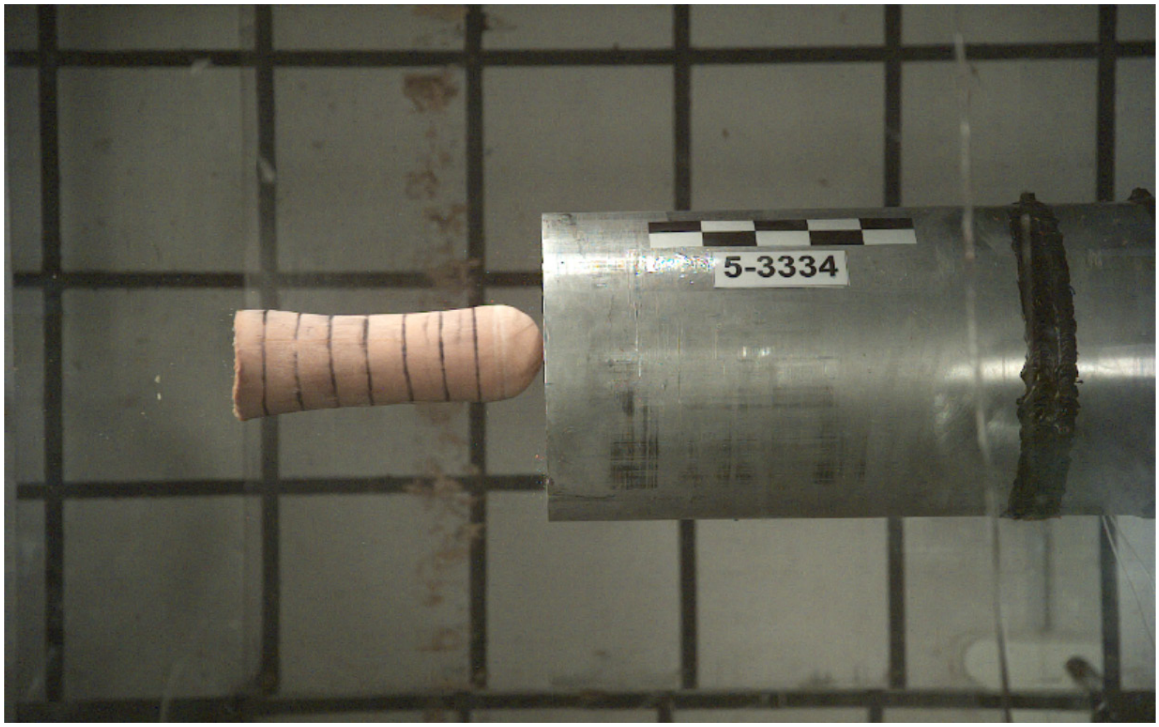

Figure A.20.—Image 5-3334 side view.

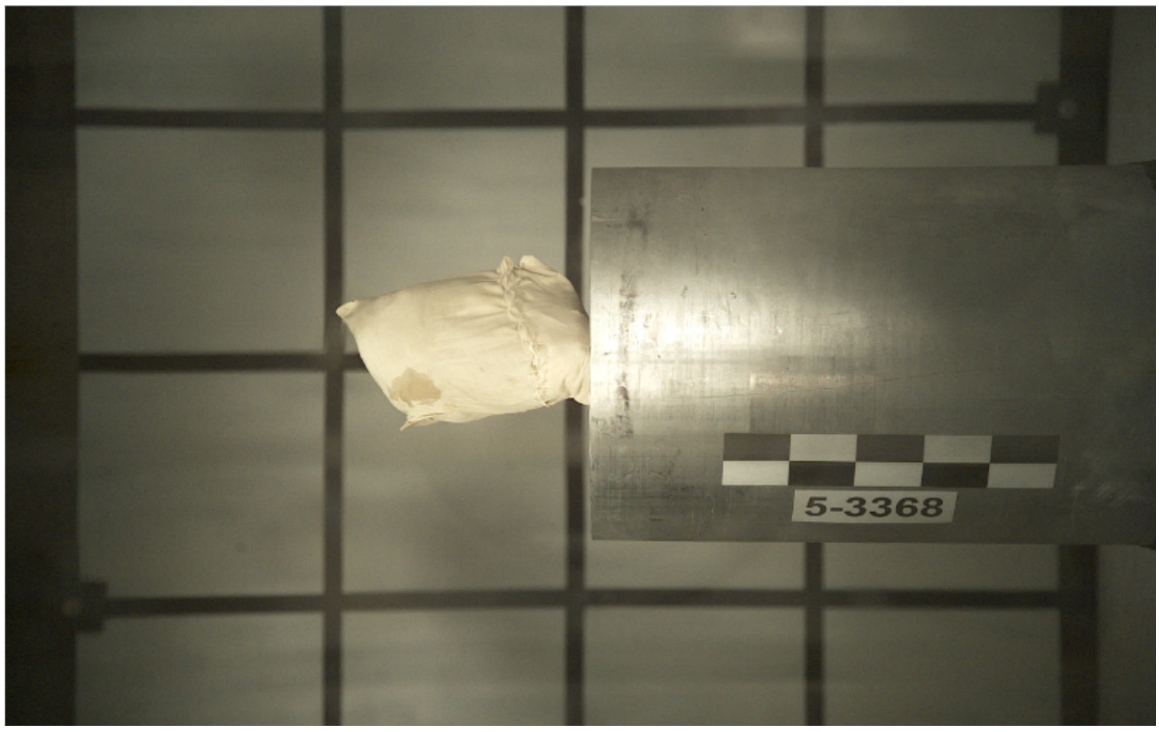

Figure A.21.—Image 5-3368 top view.

Figure A.22.—Image 5-3368 side view.

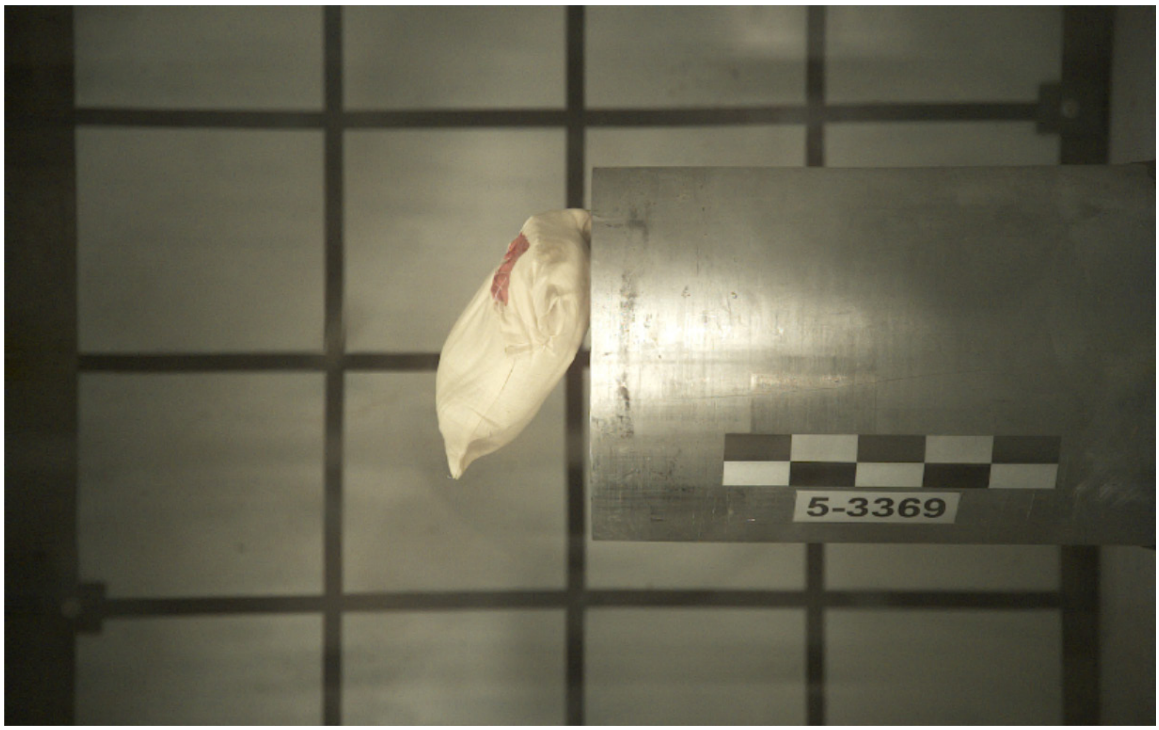

Figure A.23.—Image 5-3369 top view.

Figure A.24.—Image 5-3369 side view.

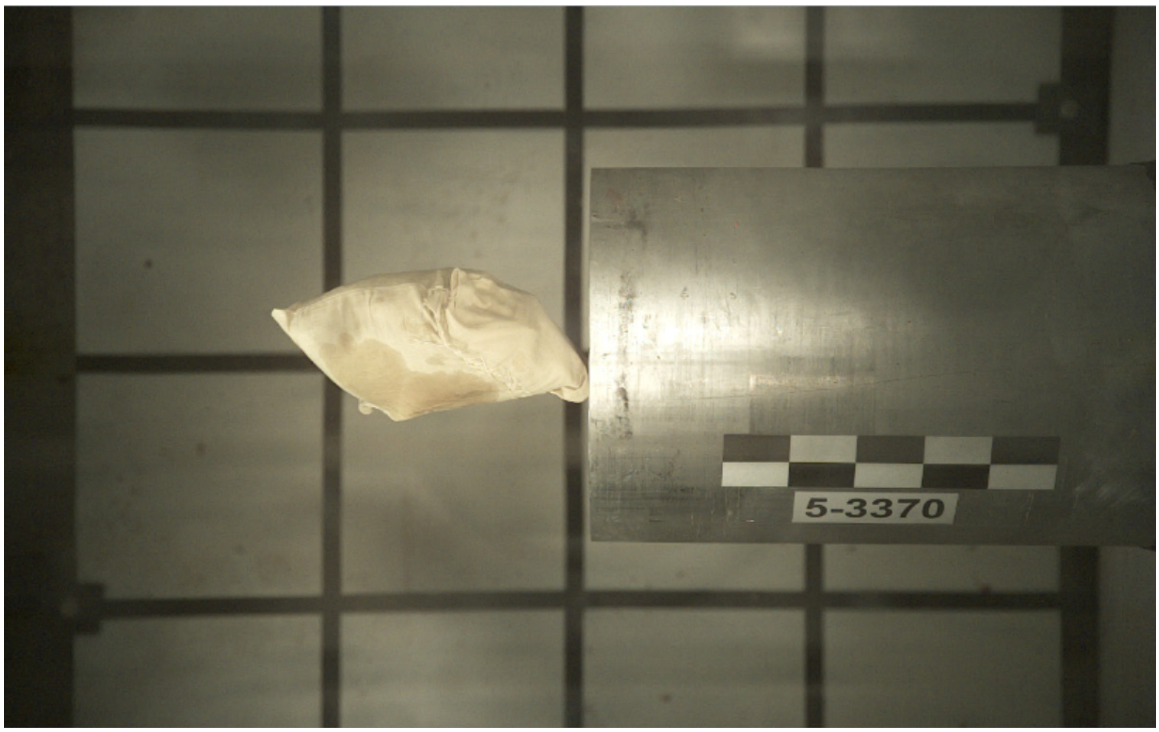

Figure A.25.—Image 5-3370 top view.

Figure A.26.—Image 5-3370 side view.

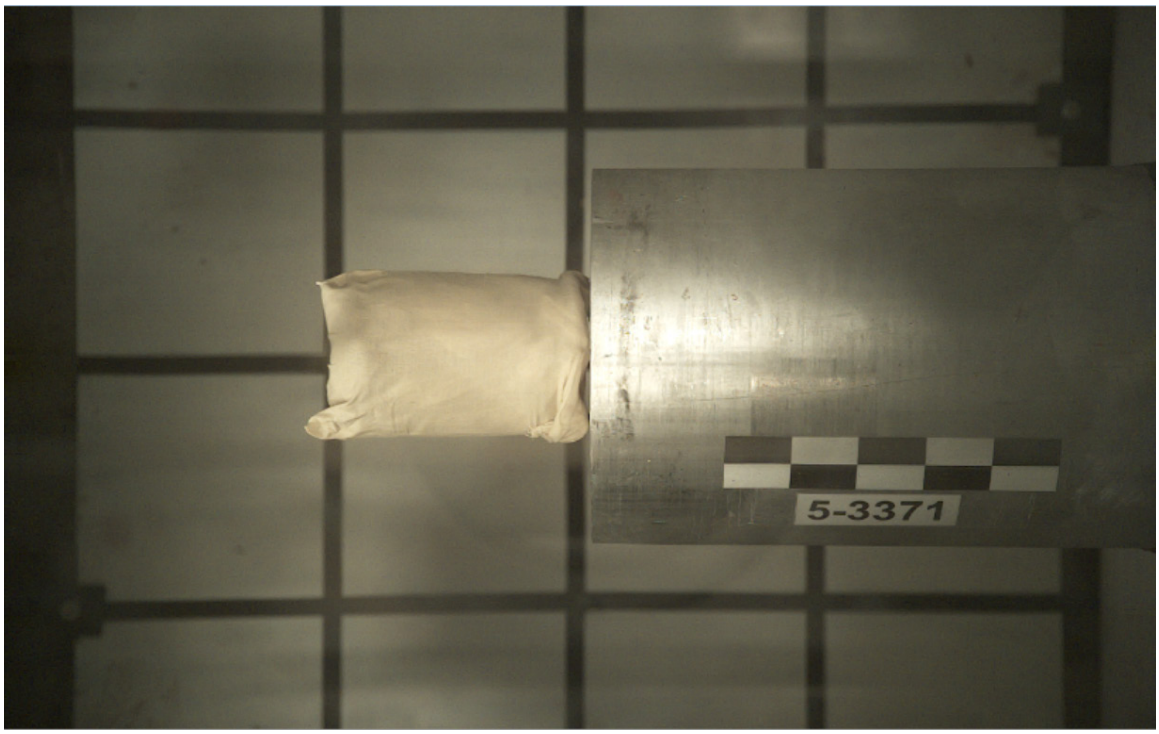

Figure A.27.—Image 5-3371 top view.

Figure A.28.—Image 5-3371 side view.

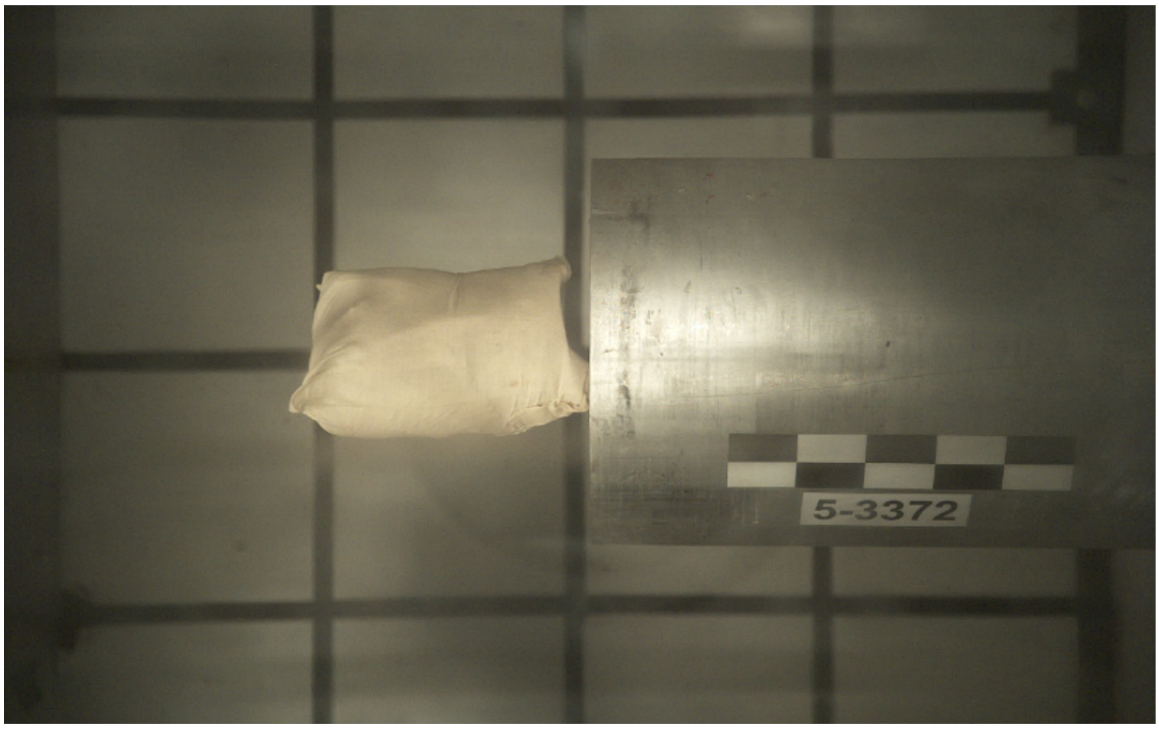

Figure A.29.—Image 5-3372 top view.

Figure A.30.—Image 5-3372 side view.

Figure A.31.—Image 5-3373 top view.

Figure A.32.—Image 5-3373 side view.

Figure A.33.—Image 5-3374 top view.

Figure A.34.—Image 5-3374 side view.

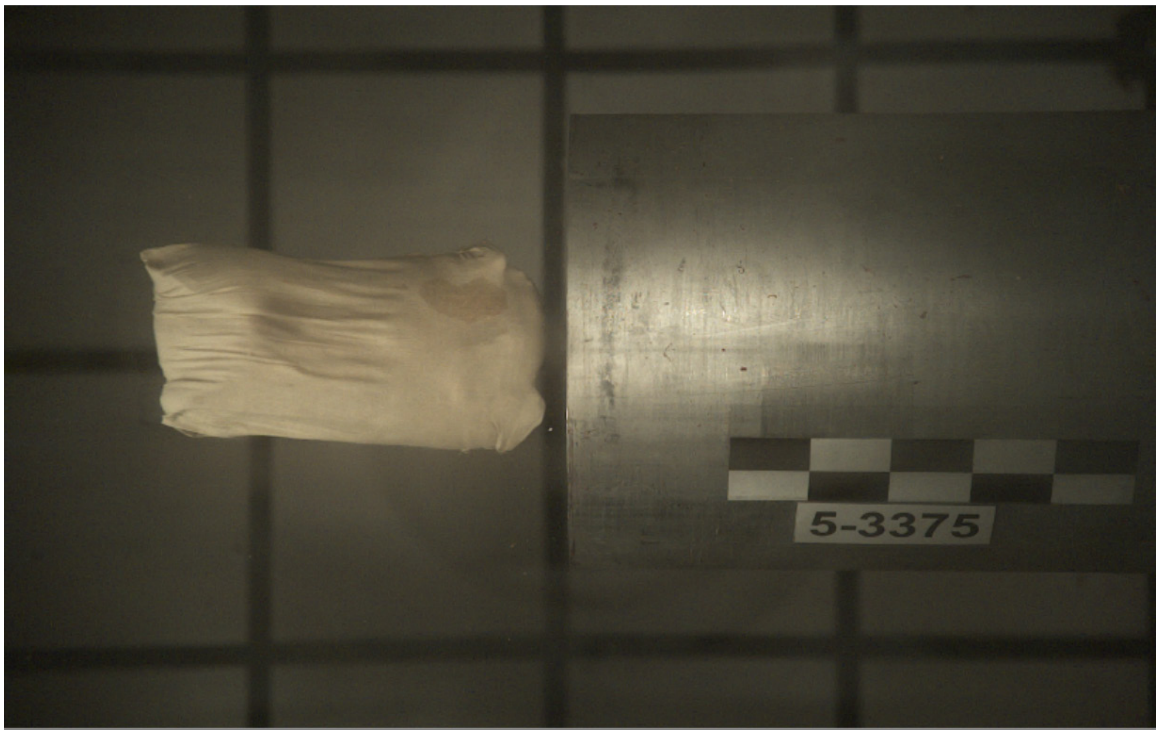

Figure A.35.—Image 5-3375 top view.

Figure A.36.—Image 5-3375 side view.

Figure A.37.—Image 5-3376 top view.

Figure A.38.—Image 5-3376 side view.

Figure A.39.—Image 5-3377 top view.

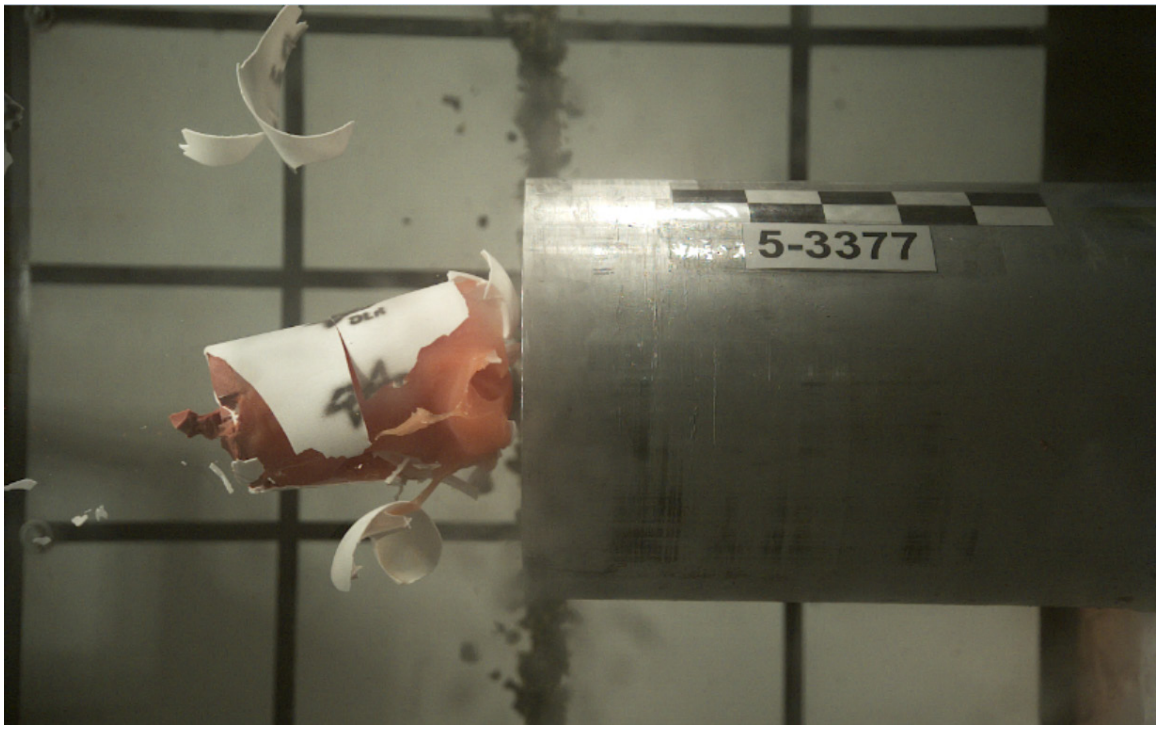

Figure A.40.—Image 5-3377 side view.

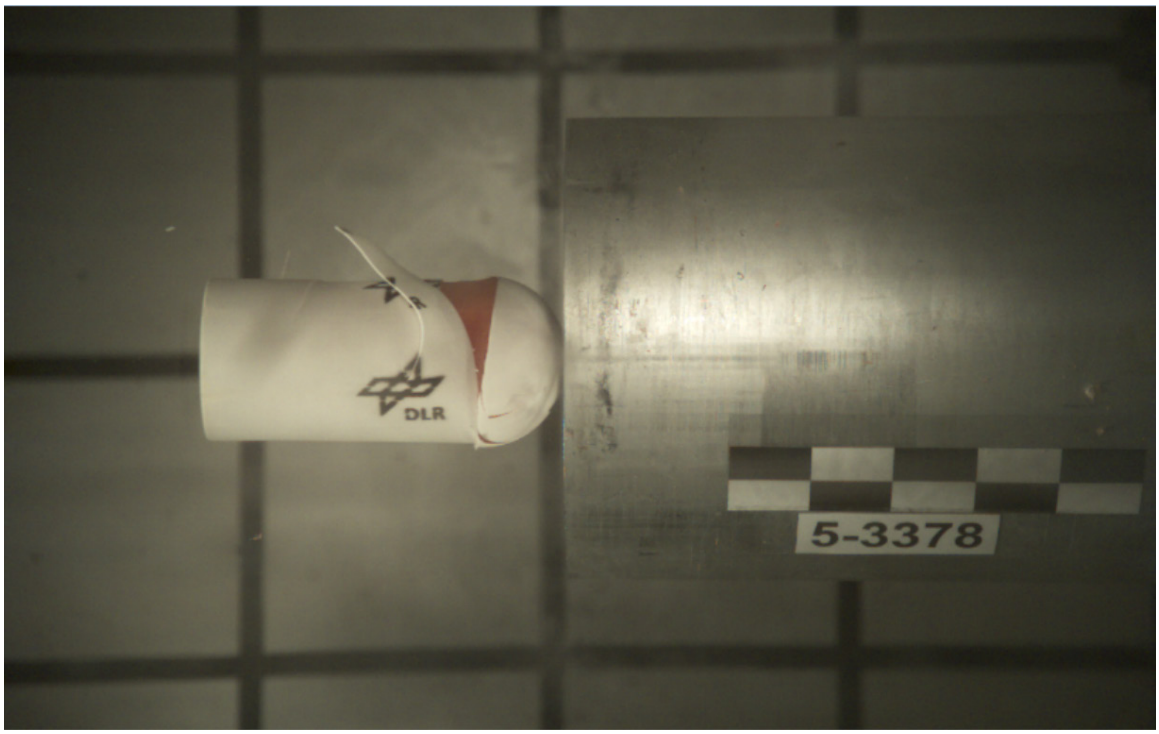

Figure A.41.—Image 5-3378 top view.

Figure A.42.—Image 5-3378 side view.

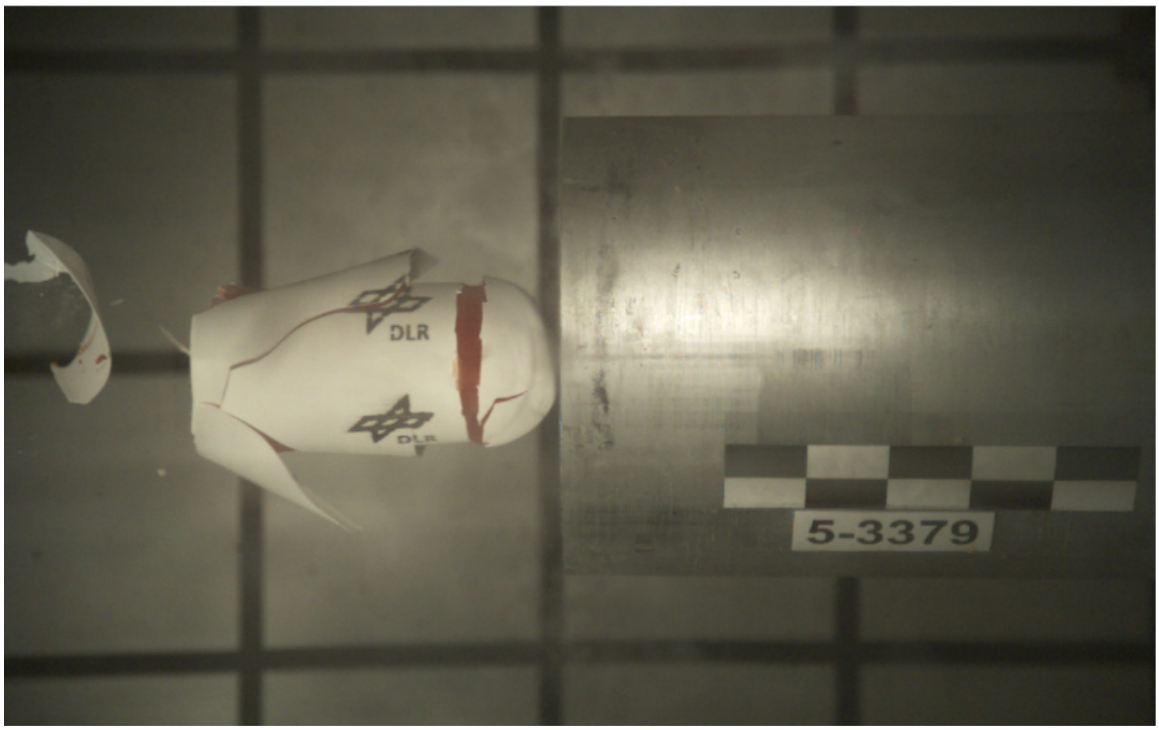

Figure A.43.—Image 5-3379 top view.

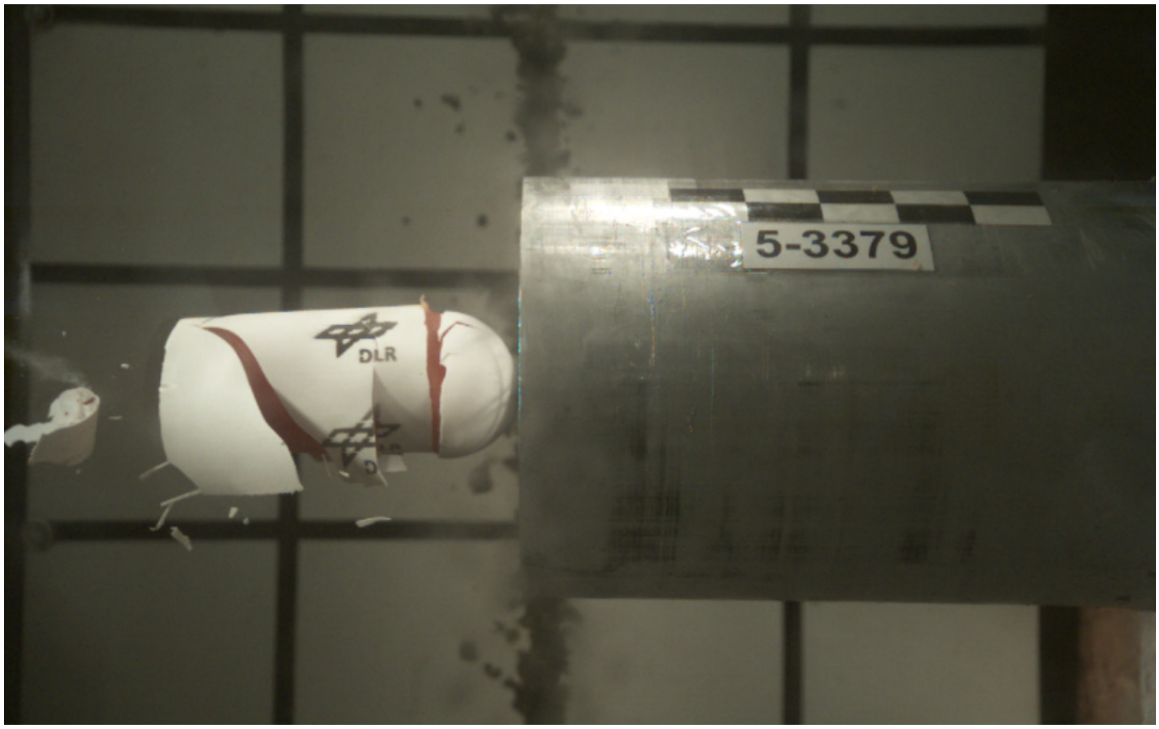

Figure A.44.—Image 5-3379 side view.

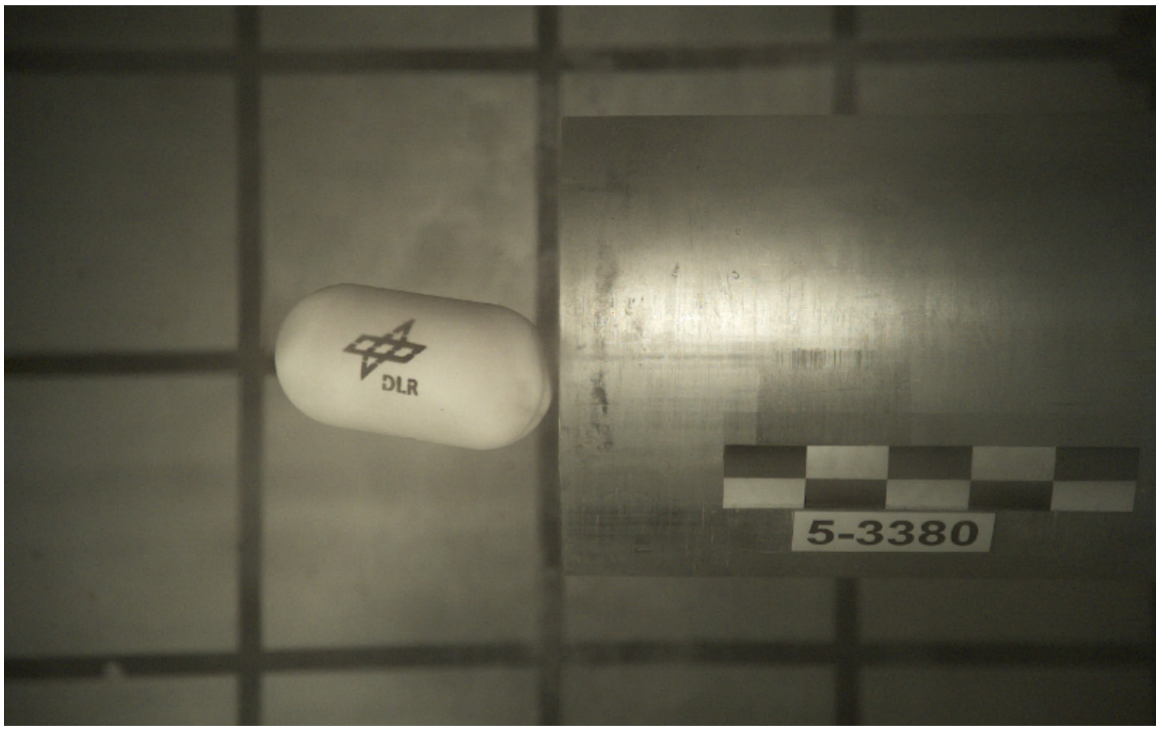

Figure A.45.—Image 5-3380 top view.

Figure A.46.—Image 5-3380 side view.

Figure A.47.—Image 5-3381 top view.

Figure A.48.—Image 5-3381 side view.

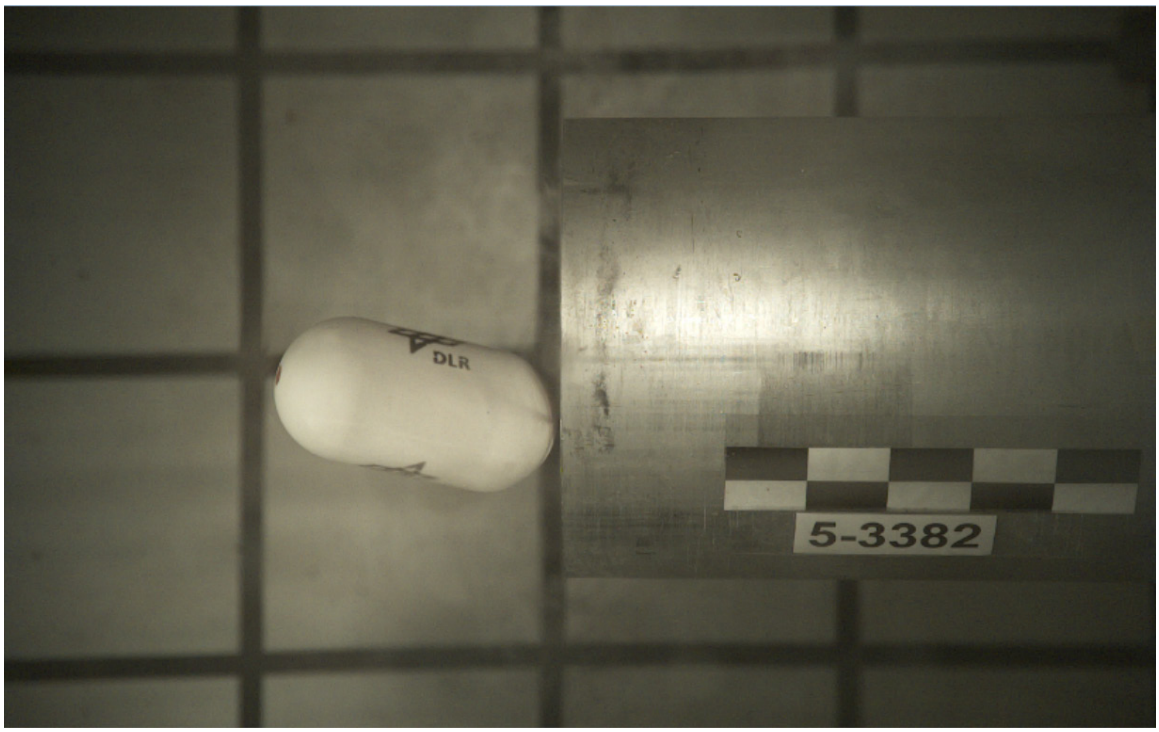

Figure A.49.—Image 5-3382 top view.

Figure A.50.—Image 5-3382 side view.

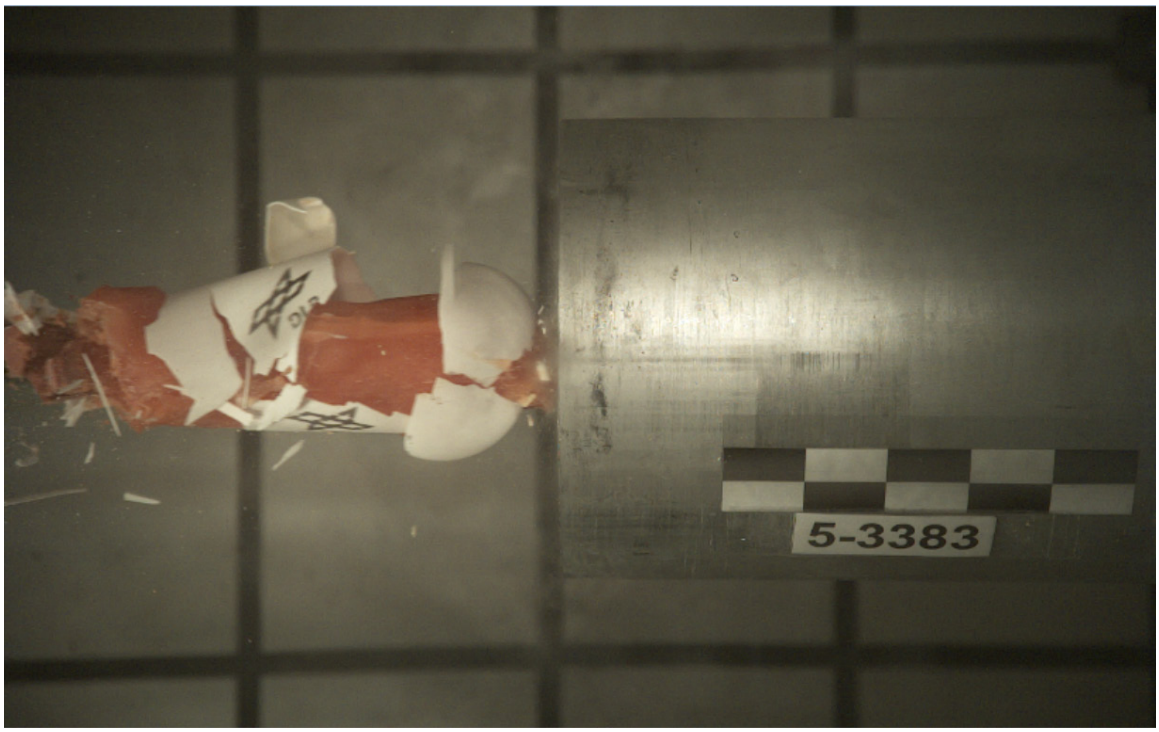

Figure A.51.—Image 5-3383 top view.

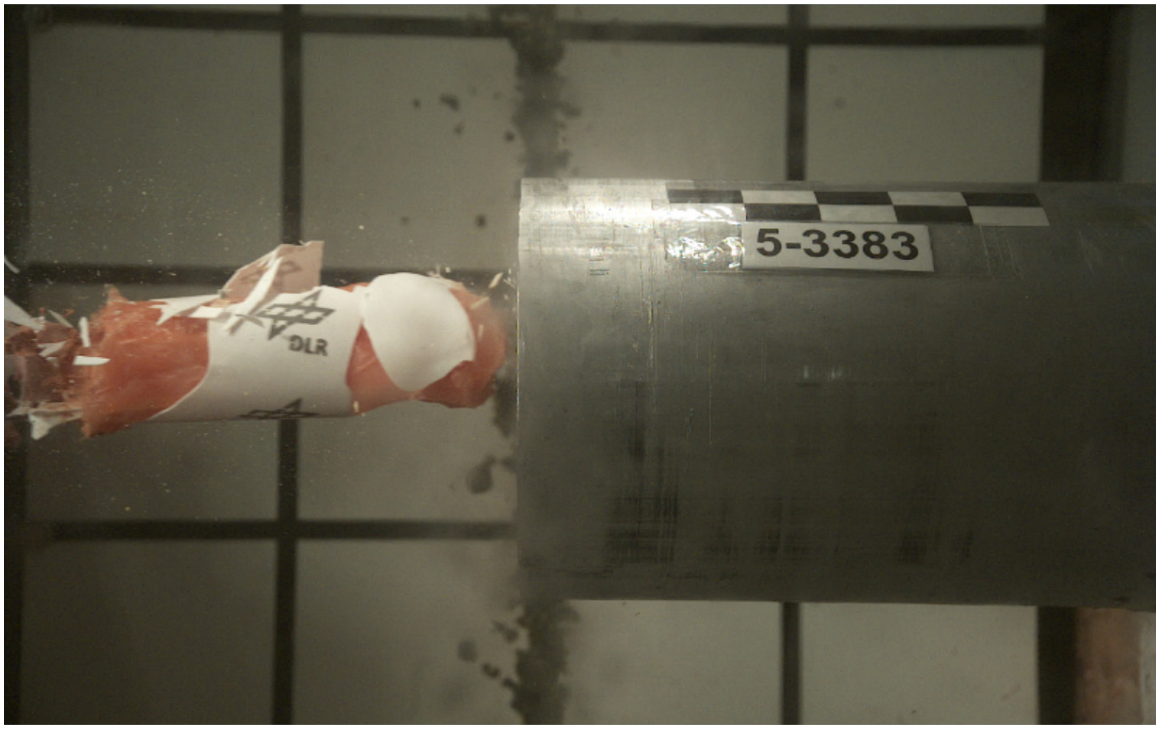

Figure A.52.—Image 5-3383 side view.

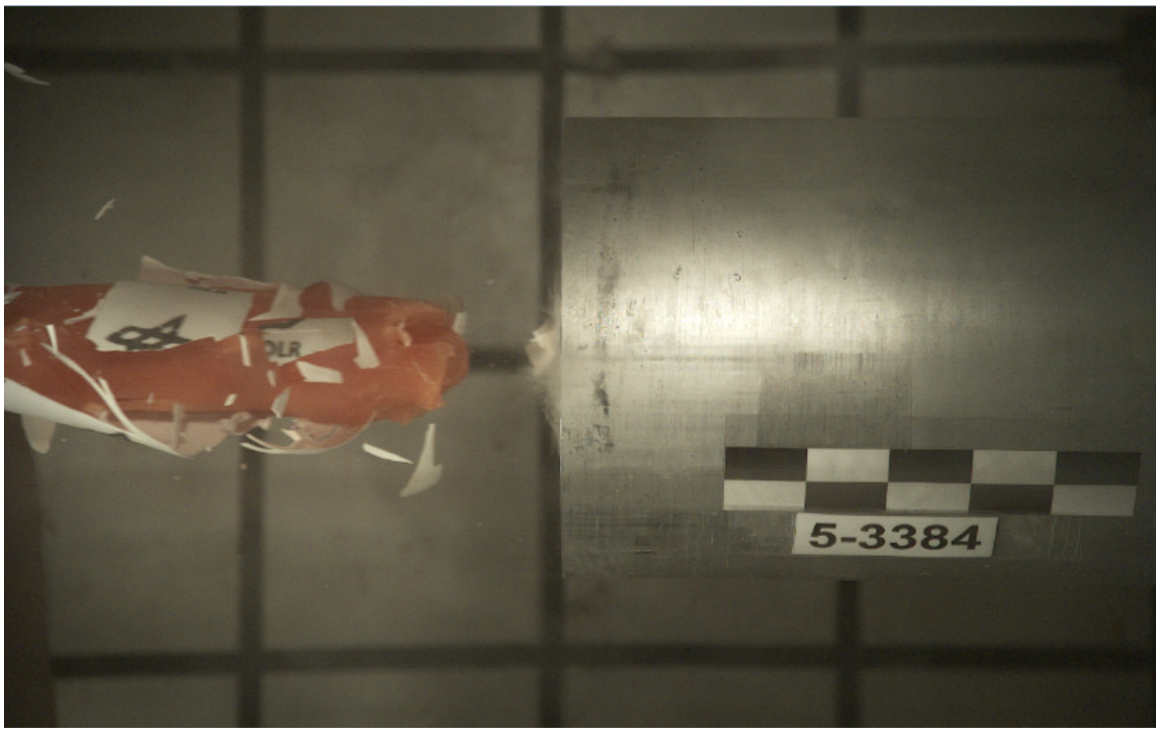

Figure A.53.—Image 5-3384 top view.

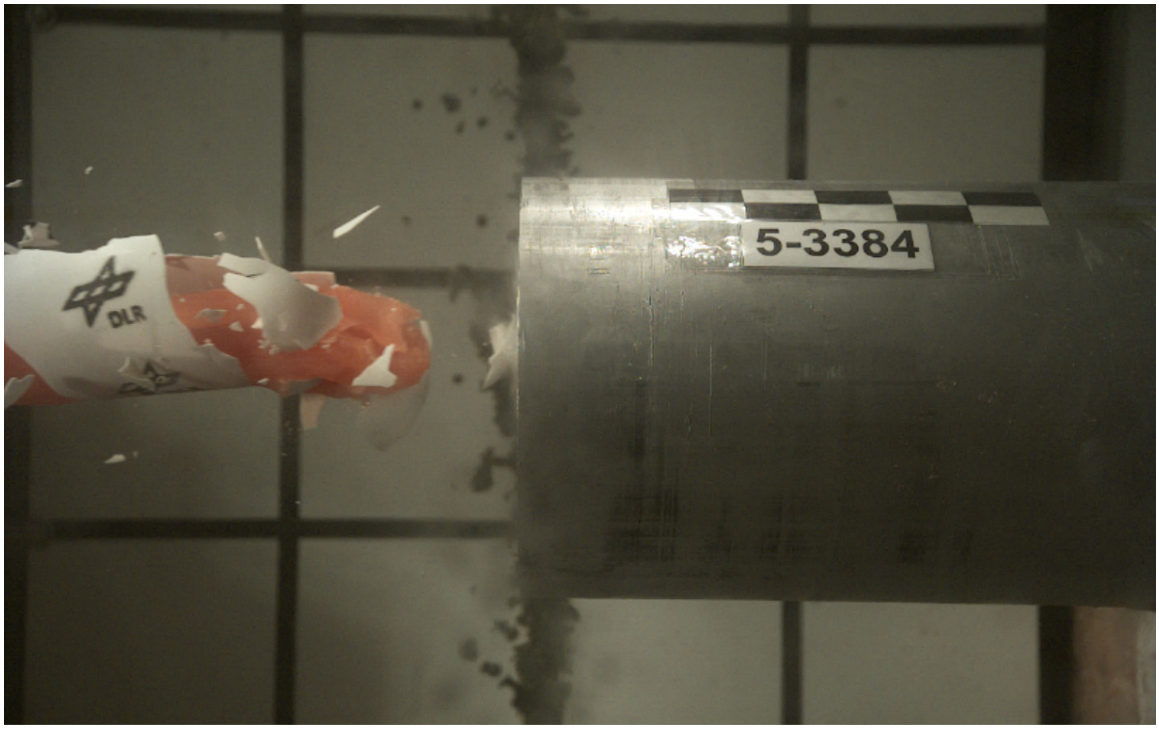

Figure A.54.—Image 5-3384 side view.

Figure A.55.—Image 5-3385 top view.

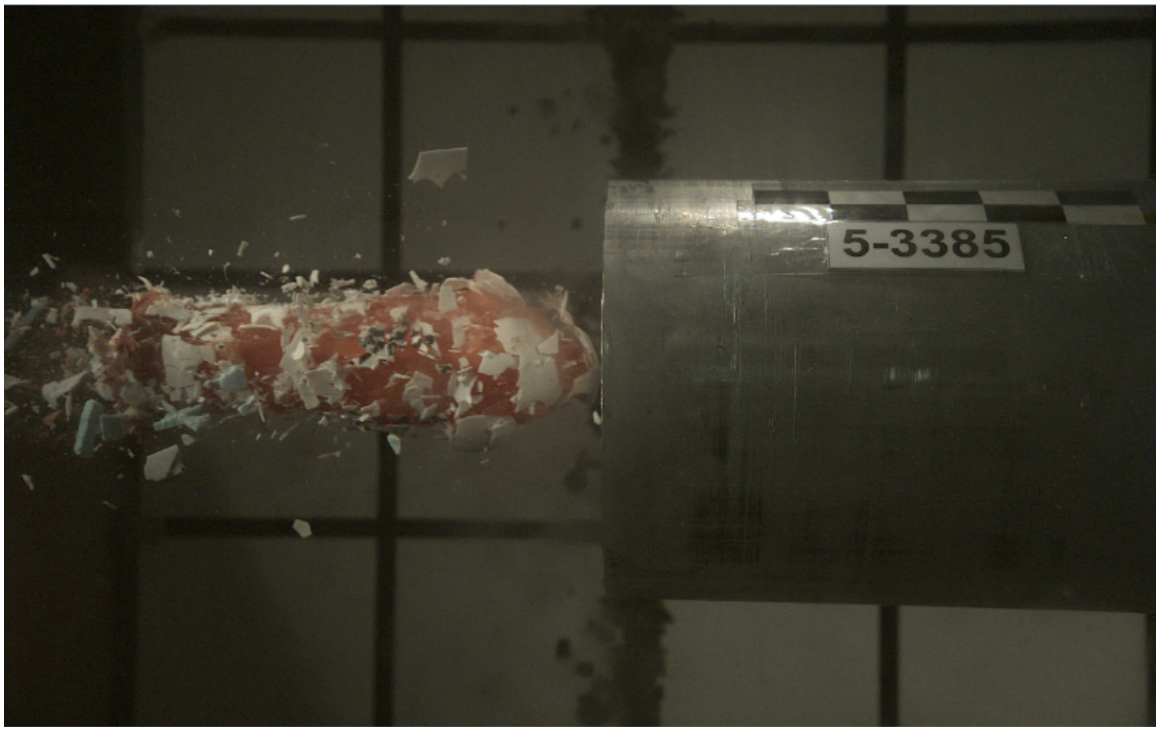

Figure A.56.—Image 5-3385 side view.

References

1. Budgey, R., The Development of a Substitute Artificial Bird by the International Birdstrike Research Group for Use in Aircraft Component Testing. International Bird Strike Committee Meeting IBSC25/WP-IE3, Amsterdam, April, 2000.
2. Peterson, R.L. and Barber, J.P., Bird Impact Forces in Aircraft Windshield Design. Air Force Flight Dynamics Laboratory Report No. AFFDL-TR-75-150. 1976.
3. Wilbeck J.S., Impact behavior of low strength projectiles. Air Force Materials Lab Report; 1978. AFML-TR-77-134.
4. Allcock, A.W.R., Collin, D.M. The development of a dummy bird for use in bird strike research. Aeronautical Research Council; 1969. CP-1071.
5. Lavoie, M.A., Gakwaya, A., Nejad Ensan, M., Zimcik, D.G. and Nandlall, D., Bird's Substitute Tests Results and Evaluation of Available Numerical Methods, Int. J. Impact Engg. 36, 2009
6. Ritt, S.A. Projectile (Original patent). WO 2010/018107 Al. 11.08.2008.
7. Ritt, S.A., Martín de la Escalera, F., Cruz, D., Toso, N., Voggenreiter, H. A damage comparison of full-scale horizontal stabiliser leading edges incorporating HLFC technology impacted by artificial and real bird. Aerospace Structural Impact Dynamics International Conference, 2025-06-10 - 2025-06-12, Seville, Spain.
8. Crashtest-Service, Biofidelic Bird, https://www.crashtest-service.com/en/biofidelic-dummy/biofidelic-animals/biofidelic-bird/
9. Ritt, S.A., Schlie, D. Comparative Studies of bird strike by dummy tests and simulations. 2. Dummy.Crashtest.Konferenz, 2022-09-08 - 2022-09-09, Muenster, Germany.
10. Barber, J.P, Taylor, H.R. and Wilbeck, J.S. Bird Impact Forces and Pressures on Rigid and Compliant Targets. Air Force Flight Dynamics Laboratory Report No. AFFDL-TR-77-60. 1978.
11. Chen X, Yin B, Tang Z, et al. Understanding the impact response of bird strikes on engine blades using a novel wedge-Hopkinson bar system. Int. J. Impact Engg. 2023;182:104782.
12. Pereira, J.M, Ritt, S.A., Poormon, K.L, Van de Waerdt, W. and Revilock, D.M. Hopkinson bar impact force measurement for application to development of an artificial bird. Int. J. Impact Engg. https://doi.org/10.1016/j.ijimpeng.2024.104951
13. Pernas-S´anchez J, Artero-Guerrero J, Varas D, et al. Artificial bird strike on Hopkinson tube device: Experimental and numerical analysis. Int. J. Impact Engg. 2020;138:103477.
14. Jiayi Li, Xiongwen Jiang, Hongjian Wei, Yue Li, Wei Zhang, Comparative investigation of shock pressure, shock duration, pressure decay time, and elastic energy of both porous gelatin and pure gelatin in shock state. Int. J. Impact Engg. 195 (2025) 105148.
15. SAE International. (2021). Standard Test Method for Measuring Forces during Normal Impact of a Soft Projectile on a Rigid Flat Surface (Standard No. AS6940).
16. Poormon, K, (2026) Soft Body Impacts on a Large Hopkinson Bar. NASA Contractor Report NASA/CR-20260000629.
17. ASTM International (2021) Standard Test Method for Bird Impact Testing of Aerospace Transparent Enclosures (ASTM F330-21). DOI: 10.1520/F0330-21
18. Barber, J.P, Taylor, H.R. and Wilbeck, J.S., Characterization of Bird Impacts on a Rigid Plate: Part I, Air Force Flight Dynamics Laboratory Report No. AFFDL-TR-75-7, 1975.
19. Bauer, D.P. and Barber, J.P., Experimental Investigation of Impact Pressures Caused by Gelatin Simulated Birds and Ice, University of Dayton, Technical Report UDR-TR-79-114, 1979.